UNIVERSITY OF CALIFORNIA
RIVERSIDE

Microstructural Engineering for Strength and Stability in Magnesium Alloy Systems

A Dissertation submitted in partial satisfaction
of the requirements for the degree of

Doctor of Philosophy

in

Mechanical Engineering

by

Heather Katelin Salvador

September 2021

Dissertation Thesis Committee:
Dr. Suveen Mathaudhu, Chairperson
Dr. Masaru Rao
Dr. Reza Abbaschian

The Dissertation of Heather Salvador is approved:

_____

_____

_____

Committee Chairperson

University of California, Riverside

ACKNOWLEDGEMENT

To all those pushing me forward, yet there with open arms when I fall back.

ABSTRACT OF THE DISSERTATION

Microstructural Engineering for Strength and Stability in Magnesium Alloy Systems

by

Heather Katelin Salvador

Doctor of Philosophy, Mechanical Engineering
University of California, Riverside, September 2021
Dr. Suveen Mathaudhu, Chairperson

The transportation industry currently contributes to roughly one-third of greenhouse gas emissions in the United States providing a large target for innovative solutions in fuel reduction technology. One such strategy is through weight reduction which contributes to improved fuel efficiency and leads to reduced carbon emissions. Magnesium and magnesium alloys provide an encouraging prospect as a light-weight structural material with a density lower than aluminum, and high specific strength and stiffness. Unfortunately, magnesium alloys exhibit poor bulk strength and formability which hinder the adoption of magnesium on a larger scale and limits the potential applications. One solution to improving strength is via grain refinement, which has allowed magnesium strengths to reach levels not previously seen, however, maintaining the fine grain sizes and resulting strength is difficult as magnesium exhibits poor thermal stability against grain growth at low homologous temperatures. The research on understanding the fundamental mechanisms of strength as a function of reducing grain size is currently limited, and those studies that do exist note a deviation from expected strengthening trends at grain sizes as large as 1-5μm. This dissertation examines three different Mg alloy systems across the grain size regimes in which

these deviations appear to occur, focusing on strengthening mechanisms and thermal stability.

As an introduction, the claim by another author of extreme strengthening contributions from the presence of nano-spaced stacking faults in a hot-rolled magnesium alloy is supported by ruling out any significant contribution from basal texture. The second study explores the need to amend current strengthening models to accommodate grain-boundary strengthening as a function of grain size. A Mg-YH_2 metal-matrix composite was used to demonstrate the increasing degree of discrepancy between predicted strength and experimental strength with decreasing grain size. This discrepancy is shown to be reduced when applying Hall-Petch coefficients based on the presenting grain size of the system. Lastly, a Mg-Li-Ca alloy displayed hardness up to 92HV and pushed the current window for thermal stability in Mg-Li systems up to 150°C. This was accomplished using grain boundary and dispersions for strengthening, and the second-phase particles also contributed to Zener pinning and grain boundary drag leading to enhanced stability.

Contents

List of Figures

List of Tables

Chapter 1 - Introduction

Magnesium is not a material that typically comes to mind when imagining structural materials, but the benefit to magnesium lies in its specific strength. Despite this high specific strength, magnesium exhibits low bulk strength, preventing the material from gaining more widespread use. This presents an opportunity for researchers to expand the magnesium design space and available applications by increasing the strength of the metal and its alloys. Currently, high strength magnesium alloys reach ultimate tensile strengths of 400 MPa in commercially available wrought magnesium alloys, and 740 MPa in a Mg-Cu-Y alloy processed by rapidly solidified powder and extrusion [1]. Table 1-1 lists the ultimate tensile strengths and elongation at break of commercially available magnesium alloys and research alloys via nonconventional processing methods.

Table 1-1 Ultimate tensile strength and elongation to break for various magnesium alloys in varying conditions.

Alloy	Condition	UTS (MPa)	EL (%)
AM60B [2]	Cast	225-240	8-13
WE43 [3]	Cast	250	2
AZ31B [4]	Wrought	260	15
ZK60A [5]	Wrought	365	11
Elektron 675 [6]	Wrought	407	9
Mg-Gd	Extrusion + ageing	508	2.5
Mg-Gd-Y-Zr [7]	Rotary swaging + aging	710	4.5
Mg-Cu-Y [8]	Rapidly solidified powder + extrusion	740	1.8

Each of these examples involve a form of severe plastic deformation processing for microstructural refinement and precipitation strengthening for material property

improvement. Among the various strategies currently employed within magnesium strengthening research, more recent attention has been given toward understanding the strengthening effect and dislocation interactions as a function of domain size. The most commonly studied domain is grain size, estimated to provide strengthening as characterized by the Hall-Petch relation:

$$\sigma_y = \sigma_0 + {}^{k}/_{\sqrt{d}}$$

Where σ_0 is the lattice friction term, k is an empirical constant, and d is grain size.

There is a plethora of physical models that have been proposed to explain the underpinning mechanisms responsible for the Hall-Petch relation. In the dislocation pile-up model, dislocations encounter grain boundaries as obstacles. Further plasticity is only possible when the stress accumulation at the head of the dislocation pile-up surpasses the stress required to nucleate a dislocation source in the neighboring grain. Another model proposes grain boundaries themselves to be the source of dislocation emission, with increased GB stress concentrations or ledges available for emission with smaller grains. The model on geometrically necessary dislocations explains strengthening via normal dislocation slip followed by the formation of geometrically necessary dislocation once uniform deformation is no longer possible beyond a certain dislocation density. The mean slip distance model relates the strengthening to the grain area available for slip to occur, and as such the grain size affects the dislocation density. Despite the variety of models proposed, there remains a lack of evidence, experimentally or theoretically, that conclusively validate any of these approaches over another, and the mechanism doesn't seem to be consistent between different crystal structures. A few issues set forth in

studying the Hall-Petch relation involves the difficulty in creating nanoscale materials without artefacts and unclear understanding of overlapping strengthening mechanisms that occur at smaller domain sizes.

Li et al. aggregated the available data for strength as a function of grain size and found a wide spread of experimental reported values for the Hall-Petch constant, leading the author to question if the Hall-Petch relation was optimum to describe strengthening at small length scales[9]. In fact, it was noted that the experimental data fit better to a generalized size-dependence equation applicable to domain sizes where dislocation source sizes are constrained. Further, a review by Meyers et al. showed the apparent deviation and reversal of the typical Hall-Petch trend in a variety of materials [10]. This has been explained as a transition from dislocation-mediated plasticity to grain-boundary sliding below a critical grain size where the grain area is too small to provide dislocation activity, and termed the inverse Hall-Petch relation. Choskshi et al. first reported the inverse Hall-Petch effect in nanocrystalline Cu and Pd when grain sizes are less than 16nm or 14nm [11], and Erb et al. showed a Hall-Petch breakdown in Ni with grain sizes below 10nm [12].

The anisotropic nature of the HCP system further convolutes the study of plasticity across length scales. Yu et al. reviewed the factors that influence the Hall-Petch constant, k, or hardenability, in magnesium alloys, and found that texture, grain size, boundary conditions, temperature, and strain all have a large influence on k [13], which indicates the transition in dominant plasticity mechanisms. In magnesium, unlike in FCC metals, the propensity for twinning decreases with decreasing grain size, and with

twinning acting as an important deformation mode in a material with limited slip systems active at room temperature, these transitions are more sensitive to grain size [14], [15].

Although HCP materials have not been as widely studied as FCC materials in relation to Hall-Petch, emerging research has started to chart the critical grain sizes in which the Hall-Petch relation starts to break down in magnesium. Interestingly, this transition appears to occur at grain sizes much larger than what is reported in FCC materials, with a hardening breakdown beginning at ~5μm and a reversal below 1μm [16]–[18]. Since grain boundary strengthening occurs at relatively large grain sizes in magnesium, it opens up an opportunity to better understand the transition between deformation modes and their effect on strengthening across grain sizes. Further, most of the work done on the Hall-Petch breakdown is on pure magnesium in order to minimize secondary strengthening effects, which opens up research avenues for magnesium alloys and the interactions between multiple strengthening mechanisms across grain sizes.

Another complication in strengthening via grain refinement is the capability to maintain fine grains by preventing grain growth. Magnesium, in particular, has been shown to undergo grain coarsening at temperatures below 250°C [19]–[24], leading to a loss in strength improvements realized from grain boundary strengthening. Researchers have found some success in retaining fine grains through modification of the grain boundary character [25]–[28], pinning grain boundaries [29]–[35], and using alloying to modify stacking fault energy [36]–[38]. Each of these methodologies contribute toward modifying the critical resolved shear stresses for various slip systems to inhibit grain

boundary migration, however, there is a lack of understanding of defect interactions that control strength as a function of grain size.

To address this gap, this dissertation examines the strengthening effects as a function of domain size and secondary phases by asking the following questions;

1. How can transitions in deformation mechanisms affecting strength be incorporated into conventional strengthening models?
2. What role do secondary phases play in stabilization of grain sizes and strengthening in fine-grained magnesium?

The following chapters include three papers written for publication on three different studies on strengthening mechanisms and thermal stability domain sizes in magnesium.

The first study is an extension of work done by W.W. Jian on extreme strengthening by nano-spaced stacking faults in a hot-rolled magnesium alloy [39], [40]. In collaboration with Bhattacharrya and Agnew from the University of Virginia, the effect of textural strengthening in the hot-rolled alloy was analyzed using pole figures. The analysis determined that the weak texture intensity did not contribute significantly to the strengthening seen in Jian's study, thereby reinforcing the case for the ability of nano-spaced stacking faults to provide significant strengthening in an allegory to the ability of grains to strengthen with reduced domain size.

Next, the effect of the inverse Hall-Petch effect on current strengthening models was examined using a magnesium-based metal-matrix composite was fabricated using mechanical alloying via SPEX milling and sintering through spark plasma sintering. The sintered material exhibited grain sizes <5μm, which falls within the Hall-Petch

breakdown gran size regime. The common strengthening models used to predict strength in metal-matrix composites was applied to the system to demonstrate the disparity that arises when the possible softening from Hall-Petch breakdown and inversion is not taken into account.

Lastly, the role of secondary phases in strengthening and grain size stabilization in a lightweight Mg-Li-Ca alloy with sub-micron grain sizes was studied. The combination of the fine grain sizes and dispersion of Mg_2Ca intermetallic contribute to the high hardness levels displayed by the processed alloy. Further, the fine dispersions act to pin grain boundary mobility and retard grain growth allowing for static thermal stability up to 150°C, which is an improvement over other Mg-Li alloys that undergo grain coarsening at temperatures as low as 25°C. These findings are attributed to dispersion hardening and Zener pinning which prevent the softening from the inverse Hall-Petch effect, and provide an improved Hall-Petch hardenability capacity over the LZ91 magnesium series, and on par with the AZ31 series. This points to the potential of developing a light-weight magnesium alloy with higher hardness and improved thermal stability over other lightweight magnesium alloys.

From each of these studies, the underlying mechanisms contributing to strengthening in magnesium across fine domain sizes is studied, and the following questions are evaluated:

1. Is there a non-linear hardening trend in magnesium systems displaying a range of fine domain sizes?

2. Within these fine grain sizes, do particulate or precipitate presence affect the relative thermal stability against grain coarsening?
3. What are the relative effects of other strengthening mechanisms as a function of domain size?

References

[1] A. Kato, T. Suganuma, H. Horikiri, Y. Kawamura, A. Inoue, and T. Masumoto, "Consolidation and mechanical properties of atomized Mg-based amorphous powders," *Materials Science and Engineering: A*, vol. 179–180, pp. 112–117, May 1994, doi: 10.1016/0921-5093(94)90175-9.

[2] "Magnesium AM60B Cast Alloy (M10602)," *AZoM.com*, Jun. 14, 2013. https://www.azom.com/article.aspx?ArticleID=9237 (accessed Aug. 19, 2021).

[3] "Magnesium Elektron WE43 Alloy (UNS M18430)," *AZoM.com*, Jun. 18, 2013. https://www.azom.com/article.aspx?ArticleID=9279 (accessed Aug. 19, 2021).

[4] P. S. says, "Magnesium AZ31B Alloy (UNS M11311)," *AZoM.com*, Sep. 04, 2012. https://www.azom.com/article.aspx?ArticleID=6707 (accessed Aug. 19, 2021).

[5] "Magnesium ZK60A Alloy (M16600)," *AZoM.com*, Sep. 04, 2012. https://www.azom.com/article.aspx?ArticleID=6710 (accessed Aug. 19, 2021).

[6] "Magnesium Elektron Elektron® 675 Magnesium Wrought Alloy." http://www.matweb.com/search/datasheettext.aspx?matguid=1c5d941454cb405fbdbb6dae334ffd77 (accessed Aug. 19, 2021).

[7] R. G. Li *et al.*, "Achieving exceptionally high strength in binary Mg-13Gd alloy by strong texture and substantial precipitates," *Scripta Materialia*, vol. 193, pp. 142–146, Mar. 2021, doi: 10.1016/j.scriptamat.2020.10.052.

[8] Y. Wan *et al.*, "Bulk nanocrystalline high-strength magnesium alloys prepared via rotary swaging," *Acta Materialia*, vol. 200, pp. 274–286, Nov. 2020, doi: 10.1016/j.actamat.2020.09.024.

[9] Y. Li, A. J. Bushby, and D. J. Dunstan, "The Hall–Petch effect as a manifestation of the general size effect," *Proceedings of the Royal Society A: Mathematical, Physical and Engineering Sciences*, vol. 472, no. 2190, p. 20150890, Jun. 2016, doi: 10.1098/rspa.2015.0890.

[10] M. A. Meyers, A. Mishra, and D. J. Benson, "Mechanical properties of nanocrystalline materials," *Progress in Materials Science*, vol. 51, no. 4, pp. 427–556, May 2006, doi: 10.1016/j.pmatsci.2005.08.003.

[11] A. H. Chokshi, A. Rosen, J. Karch, and H. Gleiter, "On the validity of the hall-petch relationship in nanocrystalline materials," *Scripta Metallurgica*, vol. 23, no. 10, pp. 1679–1683, Oct. 1989, doi: 10.1016/0036-9748(89)90342-6.

[12] U. Erb, “Electrodeposited nanocrystals: Synthesis, properties and industrial applications,” *Nanostructured Materials*, vol. 6, no. 5, pp. 533–538, Jan. 1995, doi: 10.1016/0965-9773(95)00114-X.

[13] H. Yu, Y. Xin, M. Wang, and Q. Liu, “Hall-Petch relationship in Mg alloys: A review,” *Journal of Materials Science & Technology*, vol. 34, no. 2, pp. 248–256, Feb. 2018, doi: 10.1016/j.jmst.2017.07.022.

[14] X. F. Tang, S. Q. Shi, and M. W. Fu, “Interactive effect of grain size and crystal structure on deformation behavior in progressive micro-scaled deformation of metallic materials,” *International Journal of Machine Tools and Manufacture*, vol. 148, p. 103473, Jan. 2020, doi: 10.1016/j.ijmachtools.2019.103473.

[15] M. R. Barnett, “A rationale for the strong dependence of mechanical twinning on grain size,” *Scripta Materialia*, vol. 59, no. 7, pp. 696–698, Oct. 2008, doi: 10.1016/j.scriptamat.2008.05.027.

[16] R. Zheng, J.-P. Du, S. Gao, H. Somekawa, S. Ogata, and N. Tsuji, “Transition of dominant deformation mode in bulk polycrystalline pure Mg by ultra-grain refinement down to sub-micrometer,” *Acta Materialia*, vol. 198, pp. 35–46, Oct. 2020, doi: 10.1016/j.actamat.2020.07.055.

[17] H. J. Choi, Y. Kim, J. H. Shin, and D. H. Bae, “Deformation behavior of magnesium in the grain size spectrum from nano- to micrometer,” *Materials Science and Engineering: A*, vol. 527, no. 6, pp. 1565–1570, Mar. 2010, doi: 10.1016/j.msea.2009.10.035.

[18] M. M. Castro, P. H. R. Pereira, A. Isaac, T. G. Langdon, and R. B. Figueiredo, “Inverse Hall–Petch Behaviour in an AZ91 Alloy and in an AZ91–Al2O3 Composite Consolidated by High-Pressure Torsion,” *Advanced Engineering Materials*, vol. 22, no. 10, p. 1900894, 2020, doi: 10.1002/adem.201900894.

[19] X. Yang, H. Miura, and T. Sakai, “Isochronal Annealing Behavior of Magnesium Alloy AZ31 after Hot Deformation,” *Mater. Trans.*, vol. 46, no. 12, pp. 2981–2987, 2005, doi: 10.2320/matertrans.46.2981.

[20] K. Kubota, M. Mabuchi, and K. Higashi, “Review Processing and mechanical properties of fine-grained magnesium alloys,” p. 8.

[21] M. Janeček, T. Krajňák, P. Minárik, J. Čížek, J. Stráská, and J. Stráský, “Structural stability of ultra-fine grained magnesium alloys processed by equal channel angular pressing,” *IOP Conf. Ser.: Mater. Sci. Eng.*, vol. 194, p. 012022, May 2017, doi: 10.1088/1757-899X/194/1/012022.

[22] J. Čížek *et al.*, “Microstructure and thermal stability of ultra fine grained Mg-based alloys prepared by high-pressure torsion,” *Materials Science and Engineering: A*, vol. 462, no. 1, pp. 121–126, Jul. 2007, doi: 10.1016/j.msea.2006.01.177.

[23] Y. Yang *et al.*, “Effects of annealing temperature on microstructure and mechanical properties of LZ91 alloy,” *Materials Science and Technology*, vol. 36, no. 18, pp. 2010–2017, Dec. 2020, doi: 10.1080/02670836.2020.1853361.

[24] F. Guo, L. Liu, Y. Ma, L. Jiang, D. Zhang, and F. Pan, “Mechanism of phase refinement and its effect on mechanical properties of a severely deformed dual-phase Mg–Li alloy during annealing,” *Materials Science and Engineering: A*, vol. 772, p. 138792, Jan. 2020, doi: 10.1016/j.msea.2019.138792.

[25] Yu. R. Kolobov, G. P. Grabovetskaya, M. B. Ivanov, A. P. Zhilyaev, and R. Z. Valiev, “Grain boundary diffusion characteristics of nanostructured nickel,” *Scripta Materialia*, vol. 44, no. 6, pp. 873–878, Apr. 2001, doi: 10.1016/S1359-6462(00)00699-0.

[26] T. Fujita, Z. Horita, and T. G. Langdon, “Using grain boundary engineering to evaluate the diffusion characteristics in ultrafine-grained Al–Mg and Al–Zn alloys,” *Materials Science and Engineering: A*, vol. 371, no. 1, pp. 241–250, Apr. 2004, doi: 10.1016/j.msea.2003.12.042.

[27] S. Takaki, D. Akama, N. Nakada, and T. Tsuchiyama, “Effect of Grain Boundary Segregation of Interstitial Elements on Hall–Petch Coefficient in Steels,” *Mater. Trans.*, vol. 55, no. 1, pp. 28–34, 2014, doi: 10.2320/matertrans.MA201314.

[28] A. M. Jamili, A. Zarei-Hanzaki, H. R. Abedi, and P. Minárik, “The grain boundary character distribution in thermomechanically processed rare earth bearing magnesium alloy,” *Journal of Alloys and Compounds*, vol. 798, pp. 158–166, Aug. 2019, doi: 10.1016/j.jallcom.2019.04.306.

[29] F. J. Humphreys and M. G. Ardakani, “Grain boundary migration and Zener pinning in particle-containing copper crystals,” *Acta Materialia*, vol. 44, no. 7, pp. 2717–2727, Jul. 1996, doi: 10.1016/1359-6454(95)00421-1.

[30] J. Zhou *et al.*, “Zener pinning by coherent particles: pinning efficiency and particle reorientation mechanisms,” *Modelling Simul. Mater. Sci. Eng.*, vol. 25, no. 6, p. 065008, Jun. 2017, doi: 10.1088/1361-651X/aa6cfb.

[31] J. Liao, N. Yamamoto, and K. Nakata, “Effect of Dispersed Intermetallic Particles on Microstructural Evolution in the Friction Stir Weld of a Fine-Grained Magnesium Alloy,” *Metall Mater Trans A*, vol. 40, no. 9, pp. 2212–2219, Sep. 2009, doi: 10.1007/s11661-009-9921-2.

[32] A. C. Hänzi *et al.*, "Design strategy for microalloyed ultra-ductile magnesium alloys," *Philosophical Magazine Letters*, May 2009, doi: 10.1080/09500830902960125.

[33] L.-M. Wu, W.-H. Wang, Y.-F. Hsu, and S. Trong, "Effects of homogenization treatment on recrystallization behavior and dispersoid distribution in an Al–Zn–Mg–Sc–Zr alloy," *Journal of Alloys and Compounds*, vol. 456, no. 1, pp. 163–169, May 2008, doi: 10.1016/j.jallcom.2007.02.054.

[34] C. J. Tweed, B. Ralph, and N. Hansen, "The pinning by particles of low and high angle grain boundaries during grain growth," *Acta Metallurgica*, vol. 32, no. 9, pp. 1407–1414, Sep. 1984, doi: 10.1016/0001-6160(84)90086-5.

[35] S. P. Ringer, W. B. Li, and K. E. Easterling, "On the interaction and pinning of grain boundaries by cubic shaped precipitate particles," *Acta Metallurgica*, vol. 37, no. 3, pp. 831–841, Mar. 1989, doi: 10.1016/0001-6160(89)90010-2.

[36] X. K. Zhang, X. Y. Yang, W. Chen, J. Qin, and J. P. Fouse, "Effect of stacking fault energy on mechanical properties and annealing behavior of brasses," *Journal of Alloys and Compounds*, vol. 679, pp. 400–407, Sep. 2016, doi: 10.1016/j.jallcom.2016.04.083.

[37] L. Tang, Y. Zhao, R. K. Islamgaliev, R. Z. Valiev, and Y. T. Zhu, "Microstructure and thermal stability of nanocrystalline Mg-Gd-Y-Zr alloy processed by high pressure torsion," *Journal of Alloys and Compounds*, vol. 721, pp. 577–585, Oct. 2017, doi: 10.1016/j.jallcom.2017.05.164.

[38] S. Komura, Z. Horita, M. Nemoto, and T. G. Langdon, "Influence of stacking fault energy on microstructural development in equal-channel angular pressing," *Journal of Materials Research*, vol. 14, no. 10, pp. 4044–4050, Oct. 1999, doi: 10.1557/JMR.1999.0546.

[39] W. W. Jian *et al.*, "Ultrastrong Mg Alloy via Nano-spaced Stacking Faults," *Materials Research Letters*, vol. 1, no. 2, pp. 61–66, Jun. 2013, doi: 10.1080/21663831.2013.765927.

[40] W. W. Jian *et al.*, "Physics and model of strengthening by parallel stacking faults," *Appl. Phys. Lett.*, vol. 103, no. 13, p. 133108, Sep. 2013, doi: 10.1063/1.4822323.

Chapter 2 - Textural and grain size contributions to strengthening in a Mg-RE alloy with nano-spaced stacking faults

H.K. Salvador[1], J.J. Bhattacharrya[2], Y. Zhu[3], S. Agnew[2], S. Mathaudhu[1]

[1]University of California, Riverside

[2]University of Virginia

[3]North Carolina State University

Abstract

Recent studies have shown promising results in the use of stacking fault and planar boundaries for providing both strengthening and plasticity pathways. One study in particular showed the presence of nano-spaced stacking faults in a hot rolled Mg-RE alloy providing exceptional strength with retention of ductility past a certain deformation point. However, while other strengthening mechanisms were considered insignificant to the stacking fault strengthening, the contribution of basal texture was not addressed. In this study, we demonstrate that the strong basal texture strengthening component typically seen in hot rolled magnesium alloys (10-30 MRD) is significantly weakened by the presence of rare earth additions and static recrystallization (5.6 MRD). This finding dismisses basal texture as a significant contribution to strengthening in a hot rolled Mg-RE alloy with nano-spaced stacking faults, bolstering the stance that the dominant strengthening mechanism can be attributed to the stacking faults.

2.1 Introduction

Simultaneous strength and ductility have been realized by several researchers in copper systems through the use of nano-twins as planar boundaries [1]–[5]. Unlike grain boundaries, nano-twins provide a high density of planar defects that allow for both hard and soft slip mechanisms, contributing to strengthening and enhanced work hardening capability. Mechanisms to circumvent the strength-ductility paradox are especially beneficial towards systems like magnesium where limited available slip systems present inherently poor ductility. Similar to the copper studies mentioned above, Jian et al. demonstrated strengthening while minimizing the accompanying drop in ductility through the production of nano-spaced stacking faults via hot rolling [6].

The stacking faults formed in parallel along the basal planes and are thought to trap dislocations as they travel along pyramidal planes. Work hardening may be increased as gliding <c+a> dislocations cut the stacking faults causing fragmentation which leads to additional pinning sites for dislocation interaction. These proposed phenomena were observed through TEM imaging of the fracture surface post-tensile testing. From these finding, a physical model was proposed to model this strengthening which linearly relates the yield stress to the reciprocal of the mean spacing of the stacking faults in a parallel to the Hall-Petch relation [7].

While the strengthening contributions from solid solution alloying, grain refinement, and precipitates were ruled out and discounted, it was later pointed out that hot rolled magnesium alloys tend to form a strong basal textural component which could potentially provide a non-trivial contribution to the strengthening seen in Jian's study.

Therefore, this study builds upon the work done by Jian by evaluating the presence and extent of texture in the rolled Mg-RE alloy when rolled to high rolling reductions with low reductions per pass. The results show a weak textural component which is attributed to texture weakening by the rare earth additions and static recrystallization. This finding rules out texture as a dominant strengthening mechanism, supporting Jian's stance that the main contribution to the enhanced strengthening is from the nano-spaced stacking faults.

2.2 Methods and Materials

2.2.1 Material processing

Mg-8.5Gd-2.3Y-1.8Ag-0.4Zr (wt%) was cast by Qudong Wang of Shanghai Jiaotong University using the procedure found in [8]. The ingot was heat treated per the T4 schedule to dissolve precipitates and subsequently cut into strips measuring 2mm x 1mm x 7mm.

Following the processing procedure from Jian's work, the strip samples were heated to 450°C on a hot plate and held at temperature for 15 minutes prior to each rolling step. Rolling was conducted on a conventional hot roller with each pass imparting no greater than 5% reduction. Samples for further characterization were taken at 10%, 15%, 78%, and 80% rolling reductions after being allowed to air cool.

2.2.2 Sample characterization

Samples at the specified rolling reductions were mounted in acrylic and polished to a 0.05μm colloidal silica finish for all characterization steps. To gauge the strengthening effect with increasing rolling reductions, Vickers hardness indentation was

performed along the plane parallel to the rolling direction. Grain size was determined for the same plane used for hardness indentation. Analysis was conducted using the linear intercept method with visual light microscopy images. Textural pole figures for the $\{10\bar{1}0\}$, $\{0002\}$, and $\{10\bar{1}1\}$ orientations were mapped using x-ray diffraction. These figures were taken along the same plane as the hardness and grain size measurements at both the surface and again at the mid-plane of the sample.

2.3 Results and Discussion

2.3.1 Microstructural and hardness results in comparison with previous studies

The grain size was reduced from 80μm to 8μm between the 10% and 80% rolling reduction conditions respectively, similar to the 13μm achieved by Jian at 88% rolling reduction. Fig. 2-1 shows the Vickers hardness measurements which increased from 83HV at 0% rolling reduction to 108HV at 80% rolling reduction. Micrographs showing the microstructure and grain size for the 10% and 80% rolling reductions are also shown. Increasing hardness is expected with decreasing grain size, but Jian discounted grain boundaries as a significant strengthening mechanism due to the large grain size for the demonstrated strength. The micrographs also show that the precipitates from the cast condition remain dissolved throughout the rolling process.

When evaluating the similarity in degree of strengthening, the difficulty arises in comparing hardness from this study to yield strength in Jian's study, especially in magnesium where slip system activation is dependent on test direction [9], [10]. In the absence of strengthening via grain refinement and precipitation strengthening as shown in Fig. 2-1 and also ruled out by Jian, in addition to ruling out the effect of solid solution

strengthening, we are left with evaluating texture and the presence of stacking faults. The presence of stacking faults was identified in Jian's study and is assumed to have been replicated in this study, thereby leaving the evaluation of the contribution of strength from texture to explain the increase in both hardness (this study) and yield strength (Jian's study) with increased rolling reduction.

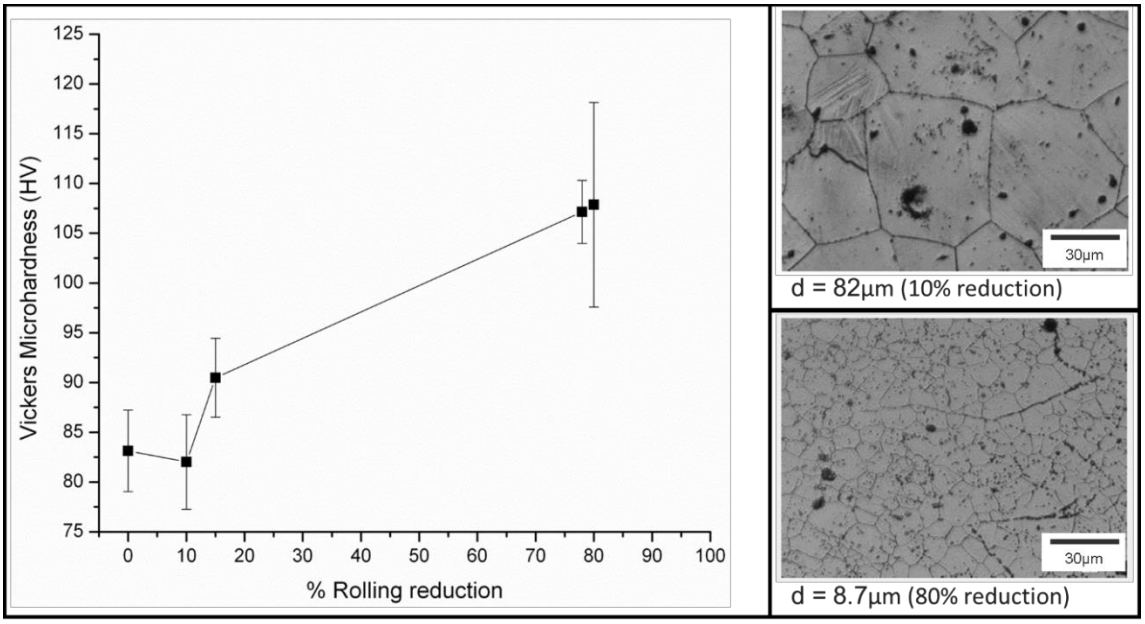

Figure 2-1 Vickers hardness vs rolling reduction and micrographs of the 10% and 80% rolling reduction conditions.

2.3.2 Texture expectations v. findings

Rolled magnesium undergoes dynamic recrystallization whereby the grains reorient for easy slip orientations in order to accommodate the rolling strain. This process forms a distinct basal texture with basal planes parallel to the rolling direction or tilted toward the rolling direction [11]. The degree of texturing is described in terms of multiples of a completely randomly oriented sample, or multiples of random orientation

(MRD). Hot rolled magnesium often reaches strong basal textural components of 10-30 MRD in pure magnesium [12]–[14], and 7-16 for AZ31 [15]–[18].

The pole figures for this study are shown in Fig. 2-2 for the {0002} basal, {10-10} prismatic, and {10-11} pyramidal orientations at both the surface of the rolled sheet as well as mid-plane to account for any variation of texture within the rolled samples. Based on what is seen in previous studies, the hot rolled texture is expected to be the most significant in the basal orientation, followed by the prismatic orientation, and then the pyramidal orientation. The results from this study follow this trend, with a weak texture shown throughout all rolling reductions in the prismatic and pyramidal orientations, and showing a more pronounced basal texture with some basal pole splitting in the mid-plane at 78% rolled reduction. While there is a definite basal texture intensity reaching a maximum of 5.6 MRD, this is still considered weak compared to the 10-30 MRD expected in rolled magnesium.

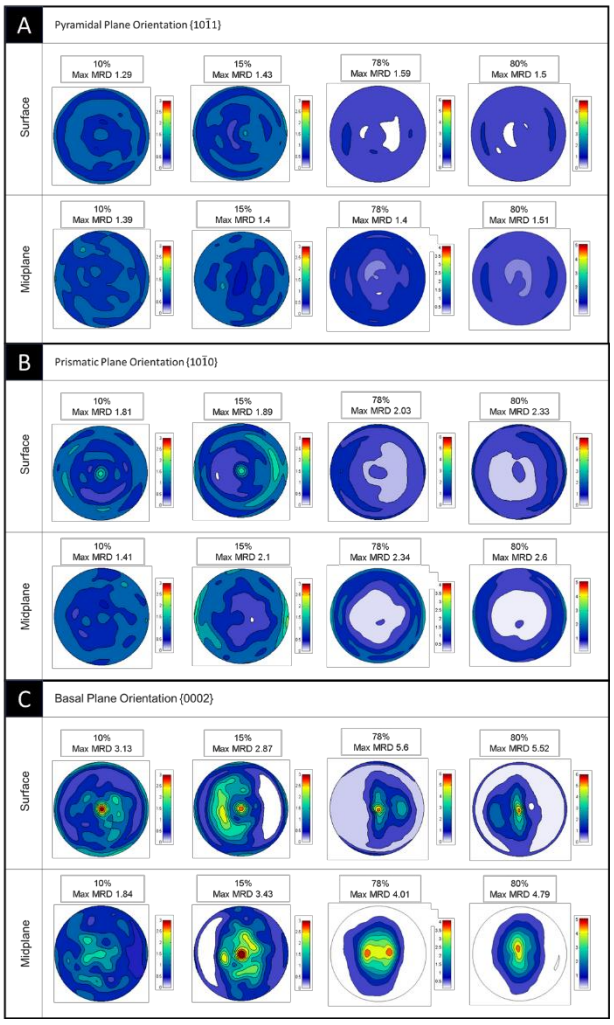

Figure 2-2 Pole figures for the A) pyramidal, B) prismatic, and C) basal plane orientations taken at the surface and midplane for samples rolled to 10%, 15%, 78%, and 80% rolling reduction. The rolling direction is along the horizontal axis, transverse direction along the vertical axis, and normal direction is out of plane.

2.3.3 Mechanisms for texture weakening

The weak texture observed in this study, combined with the steady increase in hardness with rolling reduction support the inference that textural strengthening is not a major contributor to the overall strengthening observed in this material, and can be explained by two mechanisms; rare-earth alloying additions and static recrystallization.

The addition of rare earth elements have also been shown to be effective at weakening texture [19]–[21]. This stems from their reduction of stacking fault energy [22], [23], lowering the threshold for <c+a> slip and thereby lessening the need for grains to align in order to accommodate basal slip during the rolling process. Additionally, rare earth additions tend to segregate to the higher energy grain boundaries and act as pinning mechanisms preventing grain boundary mobility, limiting the ease of reorientation to form strong textural component [24]–[26].

Static recrystallization occurred during the 450°C heating step prior to each rolling pass, easily surpassing the recrystallization temperature of 200°C for magnesium alloys [27]. Recrystallization during rolling drives the formation of basal texture as the recrystallized grains are oriented to accommodate the easy slip direction [9], [28], [29], and this process is enhanced with processing at higher temperatures. Alternatively, static recrystallization during annealing has been shown to weaken the texture formed during rolling [30]–[32], as randomly-oriented grain nucleation is more prevalent in the absence of the need to accommodation strain.

By ruling out the role of texture to strengthening, in addition to the previous explanations of the exclusion of strengthening via solid solution alloying, grain size reduction, and precipitation hardening, the main contributor to strengthening in this study, the assertation that nano-spaced stacking faults act as the dominant strengthening mechanism in Jian's study is supported.

2.4 Conclusions

A study by Jian showed extreme strengthening in a Mg-8.5Gd-2.3Y-1.8Ag-0.4Zr alloy processed by hot-rolling due to the formation of nano-spaced stacking faults. While strengthening by solid-solution additions, grain refinement, and precipitation hardening were adequately discounted, the role of texture was not addressed. In this study, the textural component was evaluated by processing Mg-8.5Gd-2.3Y-1.8Ag-0.4Zr in the same manner as Jian. The evaluated texture is similar to rolling texture seen in other magnesium alloys, however, the maximum basal pole intensity is considered weak at 5.6 MRD, where rolled magnesium typically exhibits basal pole intensities of 10-30. This weak texture is attributed to static recrystallization during reheating between rolling passes and the rare earth additions. Therefore, it is determined that basal texture is not a significant source of strengthening in this material, and further supports Jian's claim of the presence of nano-spaced stacking faults to act as a significant strengthening mechanism in this alloy.

References

[1] Y.-H. Zhao *et al.*, "Simultaneously Increasing the Ductility and Strength of Ultra-Fine-Grained Pure Copper," *Advanced Materials*, vol. 18, no. 22, pp. 2949–2953, 2006, doi: 10.1002/adma.200601472.

[2] Y. H. Zhao, Y. T. Zhu, X. Z. Liao, Z. Horita, and T. G. Langdon, "Tailoring stacking fault energy for high ductility and high strength in ultrafine grained Cu and its alloy," *Appl. Phys. Lett.*, vol. 89, no. 12, p. 121906, Sep. 2006, doi: 10.1063/1.2356310.

[3] L. Lu, Y. Shen, X. Chen, L. Qian, and K. Lu, "Ultrahigh Strength and High Electrical Conductivity in Copper," *Science*, vol. 304, no. 5669, pp. 422–426, Apr. 2004, doi: 10.1126/science.1092905.

[4] K. Lu, L. Lu, and S. Suresh, "Strengthening Materials by Engineering Coherent Internal Boundaries at the Nanoscale," *Science*, vol. 324, no. 5925, pp. 349–352, Apr. 2009, doi: 10.1126/science.1159610.

[5] M. Dao, L. Lu, Y. F. Shen, and S. Suresh, "Strength, strain-rate sensitivity and ductility of copper with nanoscale twins," *Acta Materialia*, vol. 54, no. 20, pp. 5421–5432, Dec. 2006, doi: 10.1016/j.actamat.2006.06.062.

[6] W. W. Jian *et al.*, "Ultrastrong Mg Alloy via Nano-spaced Stacking Faults," *Materials Research Letters*, vol. 1, no. 2, pp. 61–66, Jun. 2013, doi: 10.1080/21663831.2013.765927.

[7] W. W. Jian *et al.*, "Physics and model of strengthening by parallel stacking faults," *Appl. Phys. Lett.*, vol. 103, no. 13, p. 133108, Sep. 2013, doi: 10.1063/1.4822323.

[8] Q. Wang, J. Chen, Z. Zhao, and S. He, "Microstructure and super high strength of cast Mg-8.5Gd-2.3Y-1.8Ag-0.4Zr alloy," *Materials Science and Engineering: A*, vol. 528, no. 1, pp. 323–328, Nov. 2010, doi: 10.1016/j.msea.2010.09.004.

[9] S. E. Ion, F. J. Humphreys, and S. H. White, "Dynamic recrystallisation and the development of microstructure during the high temperature deformation of magnesium," *Acta Metallurgica*, vol. 30, no. 10, pp. 1909–1919, Oct. 1982, doi: 10.1016/0001-6160(82)90031-1.

[10] A. Chapuis and J. H. Driver, "Temperature dependency of slip and twinning in plane strain compressed magnesium single crystals," *Acta Materialia*, vol. 59, no. 5, pp. 1986–1994,
Mar. 2011, doi: 10.1016/j.actamat.2010.11.064.

[11] U. F. Kocks, C. N. Tomé, and H.-R. Wenk, *Texture and Anisotropy: Preferred Orientations in Polycrystals and Their Effect on Materials Properties*. Cambridge University Press, 1998.

[12] Y. Qiao, X. Wang, Z. Liu, and E. Wang, "Effect of temperature on microstructures, texture and mechanical properties of hot rolled pure Mgsheets," *Materials Science and Engineering: A*, vol. 568, pp. 202–205, Apr. 2013, doi: 10.1016/j.msea.2013.01.036.

[13] S. Biswas, D.-I. Kim, and S. Suwas, "Asymmetric and symmetric rolling of magnesium: Evolution of microstructure, texture and mechanical properties," *Materials Science and Engineering: A*, vol. 550, pp. 19–30, Jul. 2012, doi: 10.1016/j.msea.2012.03.099.

[14] G. Han, H.-K. Park, H.-K. Kim, and T.-S. Jun, "Local and global deformation behaviour in rolled pure magnesium sheets at room temperature under different strain rates," *Materials Science and Engineering: A*, vol. 762, p. 138110, Aug. 2019, doi: 10.1016/j.msea.2019.138110.

[15] D. Liu, Z. Liu, and E. Wang, "Effect of rolling reduction on microstructure, texture, mechanical properties and mechanical anisotropy of AZ31 magnesium alloys," *Materials Science and Engineering: A*, vol. 612, pp. 208–213, Aug. 2014, doi: 10.1016/j.msea.2014.06.034.

[16] S.-H. Kim, B.-S. You, C. Dong Yim, and Y.-M. Seo, "Texture and microstructure changes in asymmetrically hot rolled AZ31 magnesium alloy sheets," *Materials Letters*, vol. 59, no. 29, pp. 3876–3880, Dec. 2005, doi: 10.1016/j.matlet.2005.07.024.

[17] B. Hutchinson, M. R. Barnett, A. Ghaderi, P. Cizek, and I. Sabirov, "Deformation modes and anisotropy in magnesium alloy AZ31," *International Journal of Materials Research*, vol. 100, no. 4, pp. 556–563, Apr. 2009, doi: 10.3139/146.110070.

[18] M. Eddahbi, J. A. del Valle, M. T. Pérez-Prado, and O. A. Ruano, "Comparison of the microstructure and thermal stability of an AZ31 alloy processed by ECAP and large strain hot rolling," *Materials Science and Engineering: A*, vol. 410–411, pp. 308–311, Nov. 2005, doi: 10.1016/j.msea.2005.08.081.

[19] K. Hantzsche, J. Bohlen, J. Wendt, K. U. Kainer, S. B. Yi, and D. Letzig, "Effect of rare earth additions on microstructure and texture development of magnesium alloy sheets," *Scripta Materialia*, vol. 63, no. 7, pp. 725–730, Oct. 2010, doi: 10.1016/j.scriptamat.2009.12.033.

[20] A. Imandoust, C. D. Barrett, T. Al-Samman, K. A. Inal, and H. El Kadiri, "A review on the effect of rare-earth elements on texture evolution during processing of

magnesium alloys," *J Mater Sci*, vol. 52, no. 1, pp. 1–29, Jan. 2017, doi: 10.1007/s10853-016-0371-0.

[21] N. Stanford, "The effect of rare earth elements on the behaviour of magnesium-based alloys: Part 2 – recrystallisation and texture development," *Materials Science and Engineering: A*, vol. 565, pp. 469–475, Mar. 2013, doi: 10.1016/j.msea.2012.10.084.

[22] J. Zhang, Y. Dou, G. Liu, and Z. Guo, "First-principles study of stacking fault energies in Mg-based binary alloys," *Computational Materials Science*, vol. 79, pp. 564–569, Nov. 2013, doi: 10.1016/j.commatsci.2013.07.012.

[23] Q. Zhang, T.-W. Fan, L. Fu, B.-Y. Tang, L.-M. Peng, and W.-J. Ding, "Ab-initio study of the effect of rare-earth elements on the stacking faults of Mg solid solutions," *Intermetallics*, vol. 29, pp. 21–26, Oct. 2012, doi: 10.1016/j.intermet.2012.04.015.

[24] Z. R. Zeng *et al.*, "Texture evolution during static recrystallization of cold-rolled magnesium alloys," *Acta Materialia*, vol. 105, pp. 479–494, Feb. 2016, doi: 10.1016/j.actamat.2015.12.045.

[25] C. D. Barrett, A. Imandoust, and H. El Kadiri, "The effect of rare earth element segregation on grain boundary energy and mobility in magnesium and ensuing texture weakening," *Scripta Materialia*, vol. 146, pp. 46–50, Mar. 2018, doi: 10.1016/j.scriptamat.2017.11.004.

[26] J. D. Robson, "Effect of Rare-Earth Additions on the Texture of Wrought Magnesium Alloys: The Role of Grain Boundary Segregation," *Metall and Mat Trans A*, vol. 45, no. 8, pp. 3205–3212, Jul. 2014, doi: 10.1007/s11661-013-1950-1.

[27] A. A. Kaya, "2 - Physical metallurgy of magnesium," in *Fundamentals of Magnesium Alloy Metallurgy*, M. O. Pekguleryuz, K. U. Kainer, and A. Arslan Kaya, Eds. Woodhead Publishing, 2013, pp. 33–84. doi: 10.1533/9780857097293.33.

[28] Q. Jin, S.-Y. Shim, and S.-G. Lim, "Correlation of microstructural evolution and formation of basal texture in a coarse grained Mg–Al alloy during hot rolling," *Scripta Materialia*, vol. 55, no. 9, pp. 843–846, Nov. 2006, doi: 10.1016/j.scriptamat.2006.05.040.

[29] J. A. del Valle, M. T. Pérez-Prado, and O. A. Ruano, "Texture evolution during large-strain hot rolling of the Mg AZ61 alloy," *Materials Science and Engineering: A*, vol. 355, no. 1, pp. 68–78, Aug. 2003, doi: 10.1016/S0921-5093(03)00043-1.

[30] J. Su, A. S. H. Kabir, M. Sanjari, and S. Yue, "Correlation of static recrystallization and texture weakening of AZ31 magnesium alloy sheets subjected to

high speed rolling," *Materials Science and Engineering: A*, vol. 674, pp. 343–360, Sep. 2016, doi: 10.1016/j.msea.2016.07.107.

[31] S. A. Farzadfar, É. Martin, M. Sanjari, E. Essadiqi, and S. Yue, "Texture weakening and static recrystallization in rolled Mg–2.9Y and Mg–2.9Zn solid solution alloys," *J Mater Sci*, vol. 47, no. 14, pp. 5488–5500, Jul. 2012, doi: 10.1007/s10853-012-6440-0.

[32] Q. Huo, X. Yang, J. Ma, H. Sun, J. Wang, and L. Zhang, "Texture weakening of AZ31 magnesium alloy sheet obtained by a combination of bidirectional cyclic bending at low temperature and static recrystallization," *J Mater Sci*, vol. 48, no. 2, pp. 913–919, Jan. 2013, doi: 10.1007/s10853-012-6814-3.

Chapter 3 - Consideration of the inverse Hall-Petch trend in strengthening models for magnesium-based metal matrix composites

H.K. Salvador[1], C. Roach[1], S.N. Mathaudhu[1]

[1]University of California, Riverside

Abstract

Strengthening models hold potential for materials design by providing the ability to predict strength based off of the constituents, constituent properties prior to any material fabrication, however, the accuracy of these models needs to be improved upon for this use. In magnesium-based metal-matrix composites, Hall-Petch strengthening is often the dominant strengthening mechanism, making the need for an accurate Hall-Petch strength model imperative. The classical Hall-Petch model does not take into account the breakdown and inversion of the Hall-Petch strengthening trend, and the large grain sizes at which this occurs in magnesium necessitate consideration. In this study, the contributions of strengthening mechanisms in a magnesium-based composite with YH2 reinforcement was evaluated using current strengthening models, and found Hall-Petch strengthening to be the dominant mechanism. By employing modified Hall-Petch coefficients to include the effects of the breakdown and inverse regimes, it was found that this modified strength model more closely fits the experimental results, and is more pronounced at smaller grain sizes.

3.1 Introduction

The ability to accurately predict the mechanical properties of a metal-matrix composite based off of composition, microstructure, and processing could have a huge impact on materials design. Typical estimation methods involve summation of individual strengthening mechanism models which does not account for the interaction between active mechanisms, and lead to a huge error between the predicted and experimental yield strengths. Despite this potential error, these methods are useful in identifying the relative contributions of each strengthening mechanism. In studying the strength-ductility balance in a copper metal matrix nanocomposite, Bahador showed the relative contributions of the dominant strengthening mechanisms and found that the contributions are dependent on reinforcement and processing parameters [1]. Chen discovered the apparent presence of a transition in dominant strengthening mechanisms in an aluminum-carbon nanotube composite which was determined to be a result of the carbon nanotube aspect ratio [2]. Both Sanaty-Zadeh and Kim noted the dominance of Hall-Petch strengthening in their review of magnesium-based metal matrix composites, emphasizing the need for accurate inclusion of Hall-Petch strengthening in the models [3], [4].

As an extension of the Hall-Petch strengthening model, one could include the inverse Hall-Petch trend encompassing the tendency of experimental results to deviate and invert from the typical linear Hall-Petch trend below a critical grain size [5]. Researchers have explained this softening as a transition in the dominant deformation mode from slip-mediated to grain boundary-mediated plasticity. This transitional phenomenon previously was not explored for magnesium as the transition has been

shown to occur below 100nm [5]–[8] and fabricating magnesium at such small grain sizes was considered detrimental due to the suppression of the much needed twin deformation mode necessary for plasticity. However, experimental studies have shown the Hall-Petch breakdown and reversal to occur at grain sizes much larger than what is observed in FCC materials, pulling the range of currently studied magnesium grain sizes into the possible Hall-Petch breakdown trend.

Although there is call for modification in the current models to more accurately account for Hall-Petch strengthening, little work is aimed at further including the effect of the inverse Hall-Petch effect in these modifications. In this study, a magnesium-based metal matrix composite with YH2 particulate reinforcement processed by mechanical alloying and spark plasma sintering was used to examine the significance of the transition in deformation mechanisms affecting the Hall-Petch strength in affecting conventional strengthening models. While not exact, it was shown that by using the Hall-Petch coefficients determined by Zheng for varying grain size regimes, the predicted values more closely fit to the experimental hardness values [6].

3.2 Materials and Methods

High purity (>99.9%) Mg chips from Alpha Aesar with a particle size less than 4mm, and YH_2 chips from Strem Chemicals, Inc. with a particle size less than 0.5mm were mixed in a 9:1 magnesium to yttrium-hydride ratio by weight. The mixture was loaded within an argon glovebox, into a 440C stainless steel vial with 1/2-inch diameter 440C stainless steel balls to achieve a ball-to-powder weight ratio of approximately 5:1. The system was then cryomilled using a modified SPEX 8000D for a total of 4 hours,

operating in 5-minute cycles with a 1-minute pause between cycles. The powder was extracted from the jar within an argon glovebox, and any agglomeration was reduced using a mortar and pestle prior to sieving for collection of particles between 63μm and 125μm in size. The powder was then consolidated via SPS (Fuji Electronic SPS-211LX Spark Plasma Sintering Machine) into disks measuring 10mm in diameter by 2mm in height. Within the SPS chamber, each disk was consolidated under vacuum using 50MPa uniaxial pressure and held at a temperature of 350°C, 375°C, or 425°C for 5-minutes, and allowed to cool within the SPS chamber. The samples will be designated as follows: magnesium powder (P-M), yttrium-hydride powder (P-YH), cryomilled powder (M-MYH), Mg-YH2 disk processed at 350°C (S-350), Mg-YH2 disk processed at 375°C (S-375), $MgYH_2$ disk processed at 425°C (S-425).

The powder samples were mounted in acrylic, polished to 0.05μm colloidal silica, and coated in carbon for SEM analysis. The disks were prepared for both the hardness measurements and microstructure imaging by polishing to a 0.05μm colloidal silica finish. X-ray diffraction (Pananalytical Empyrean Series 2) with CuKα radiation was used to examine initial powder, milled powder, and consolidated disk compositions. Consolidated disk density was measured using Archimedes principle in propylene glycol. The microstructure was evaluated using scanning electron microscopy (NovaNano SEM450) at 5kV with both secondary and backscatter electron detectors. TEM foils were cut from the bulk disks using a focused ion beam (Quanta 3D 200i), and the yttrium-hydride interaction with grain boundaries was observed using transmission electron

microscopy (Tecnai T12) at 120kV. The bulk hardness properties of the disks were obtained using a Phase II Vickers machine applying a 100g load for 5-seconds.

3.3 Results

The as received powders used showed an average particulate size of 4.4 ± 7.3µm and 11.1 ± 33.9µm for magnesium and yttrium-hydride respectively. Fig. 3-1 shows the microstructure of the starting powders, milled powder, and each of the sintered conditions. It should be noted that the cryomilled powder SEM image in Fig. 3-1C was taken much later than the hardness and grain size taken immediately after cryomilling, which is what was used for analysis.

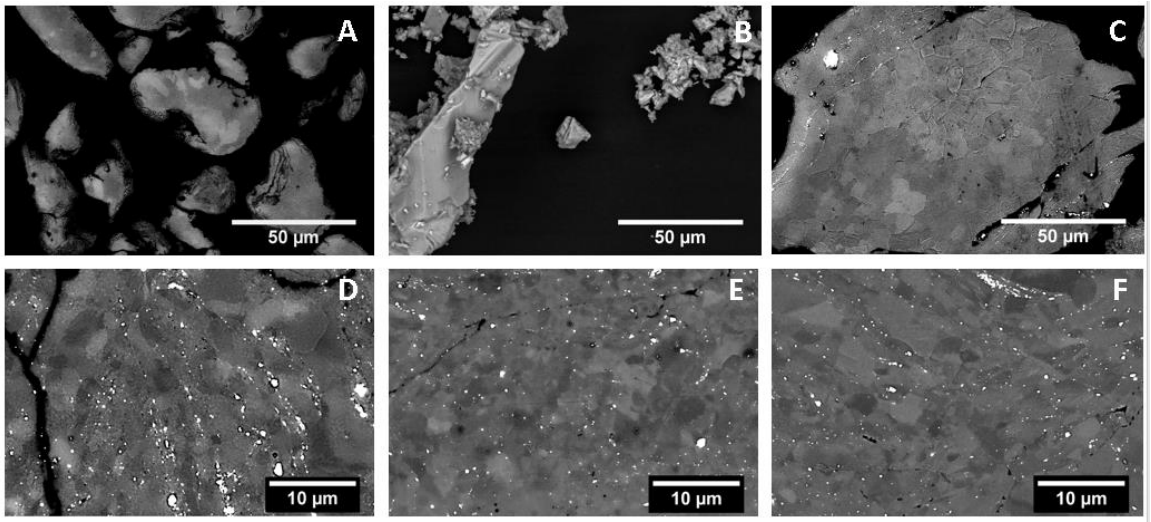

Figure 3-1 Typical microstructures of the metal-matrix composites along different stages of processing as imaged with a concentric backscatter electron ring detector in a scanning electron microscope. A) as-received magnesium powder (P-M), B) as-received yttrium-hydride powder, C) milled magnesium-yttrium-hydride metal-matrix composite particle (M-MYH), D) milled powder consolidated at 350°C (S-350), E) milled powder consolidated at 375°C (S-375), F) milled powder consolidated at 425°C (S-425).

Grain sizes increased from 141nm after milling to 4.02µm in the S-425 case, and increased with increasing sintering temperature. The Vickers hardness drops from

54.3HV after milling to 37.5 for S-350, and then again to 36.6HV for S-375 which corresponds with the increase in grain size. There is a slight increase in hardness to 40HV for S-425 despite the increase in grain size. This is most likely due to the increase in relative density of the samples with increased sintering temperature.

Table 3-1 Summary of microstructural observations and mechanical properties for as received powders, milled powders, and consolidated samples.

Sample	Grain Size (µm)	Particle Size (µm)	Volume Fraction (%)	Relative Density (%)	Hardness (HV)	Tabor's Estimate (Mpa)
Pure Mg*	-	-	-	-	30 - 45	-
YH2**	-	-	-	-	428	-
P-Mg	6.08 ± 3.54	4.4 ± 7.3	-	-	-	-
P-YH2	-	11.1 ± 33.9	-	-	-	-
M-MYH	0.141 ± 0.017	0.260 ± 0.074	1.09	-	54.3 ± 4.2	177.38
S-350	1.13 ± 0.42	0.260 ± 0.220	1.06	99.04	37.5 ± 1	122.5
S-375	3.03 ± 1.96	0.250 ± 0.210	1.23	99.56	36.6 ± 1.7	119.56
S-425	4.02 ± 1.52	0.200 ± 0.170	1.01	99.95	40 ± 2.7	130.03

* [9]–[11]
** [12]

Compositional changes between processing stages were assessed with XRD as shown in Fig. 3-2 and Fig. 3-3. The analysis shows that the M-MYH is primarily magnesium with YH_2 peaks, indicating the makeup of the metal-matrix composite.

Yttrium peaks in the P-YH2 scan disappear after milling, which is likely due to the dissolution of yttrium into the magnesium matrix, some of which contributes to the formation of a $Mg_{24}Y_5$ phase. After sintering, more yttrium is dissolved into the matrix, with the formation of another $Mg_{24}Y_5$ peak. There are no significant changes in the XRD scans between S-350, S-375, and S-425 indicating that the composite is stable between 350°C and 425°C with no detectable phase changes.

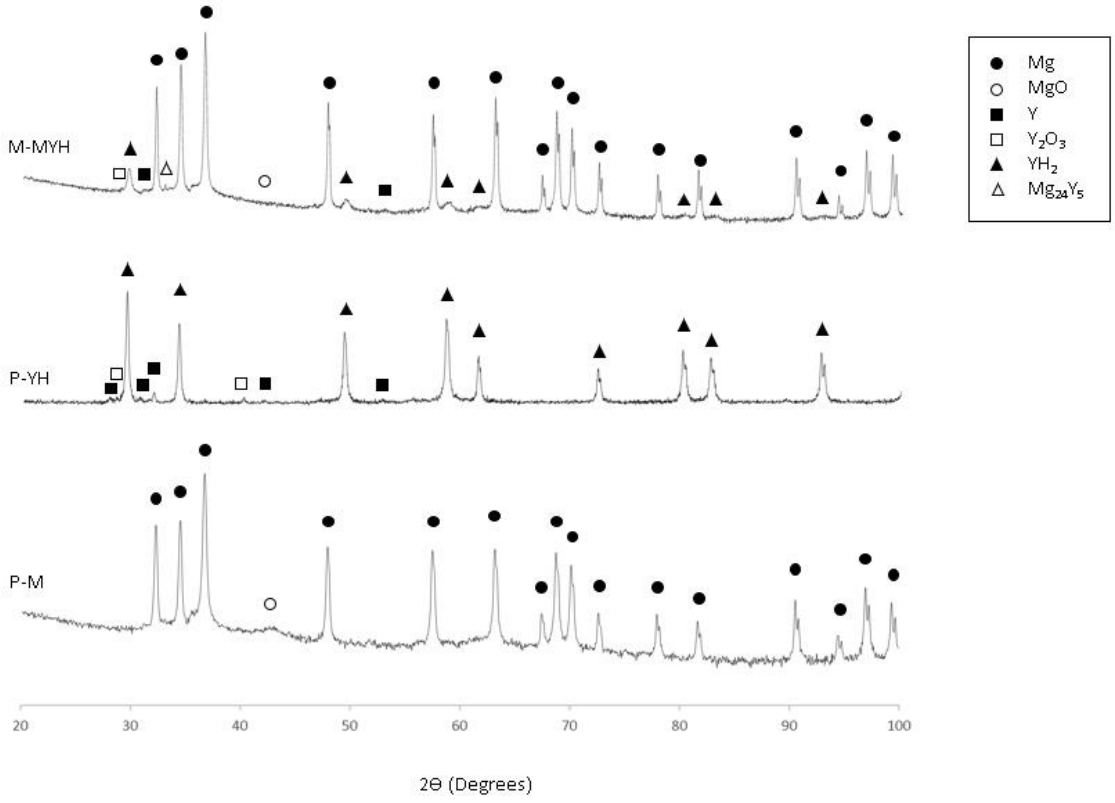

Figure 3-2 X-ray diffraction intensities of the powdered samples, P-M, P-YH, and M-MYH.

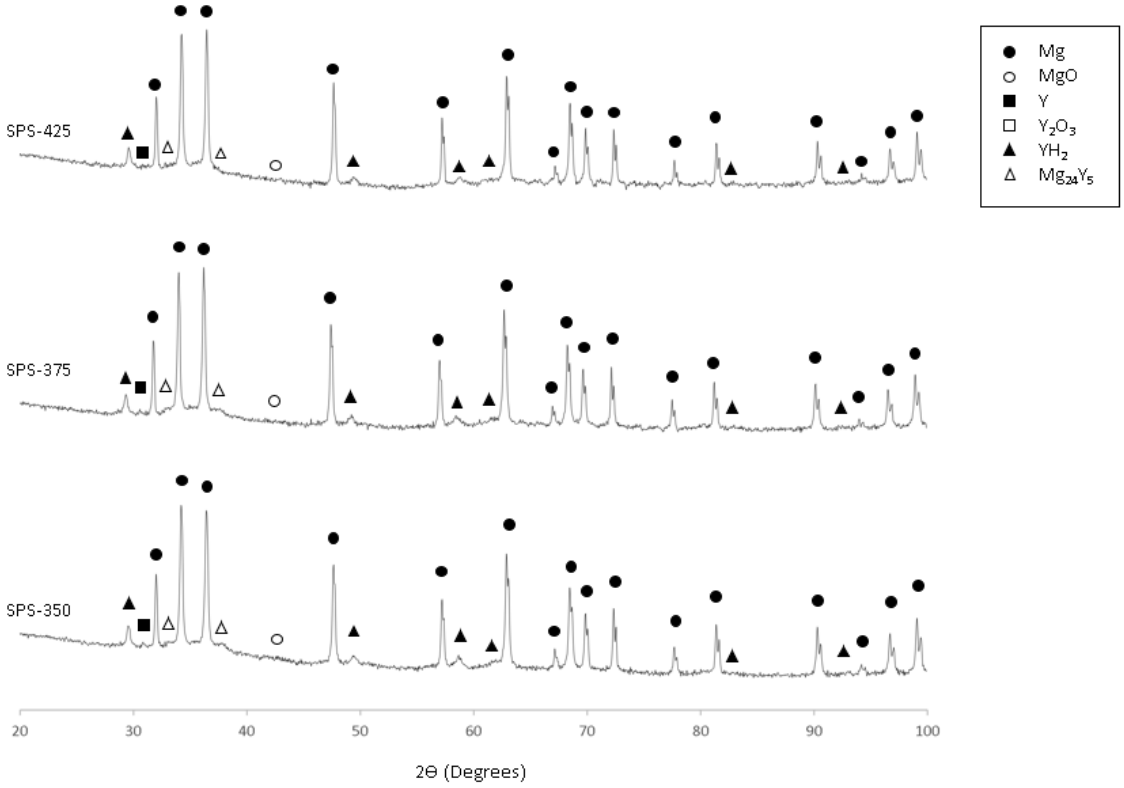

Figure 3-3 X-ray diffraction intensities for the consolidated samples, SPS-350, SPS-375, SPS-425.

Transmission electron microscopy of the S-350 sample was used to determine the size, dispersion, and coherency of the reinforcement with the matrix. The yttrium-hydride particles appear as black regions throughout the sample, and can be seen to be dispersed both within grains and at grain boundaries. Small particles along the grain boundaries can retard grain growth via Zener pinning or drag [13]–[19] which explains the lower than expected grain growth of this study in comparison with magnesium and magnesium alloys without particulate additions [20]–[23].

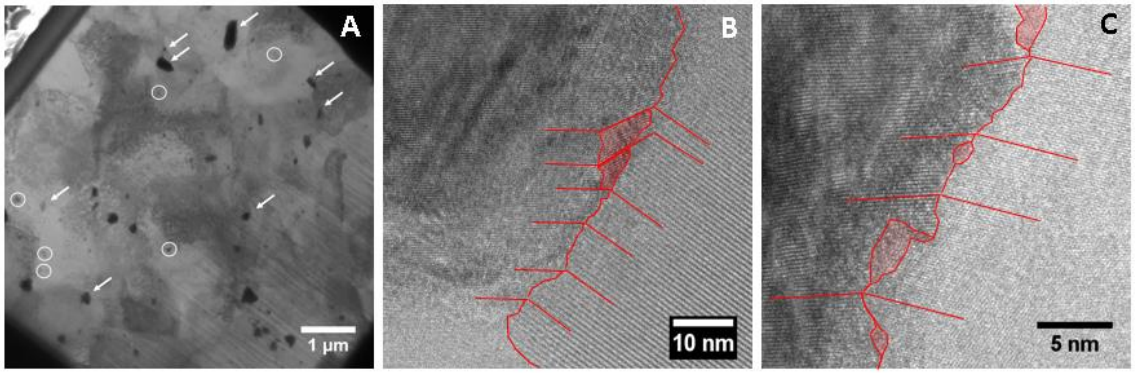

Figure 3-4 Transmission electron microscope image of the S-350 sample. A) white arrows point to particles along grain boundaries and the white circles encircle particles within grains, B)-C) HRTEM images showing coherency.

Fig. 3-4B and Fig. 3-4C show high resolution images along a particle-matrix boundary which is shown to be semi-coherent. The shaded red areas show regions of disorder indicating loss of coherence. With some areas of the particle coherent with the matrix and other areas incoherent, this particle can be considered to be semi-coherent. This coherency has effects in the performance of the metal-matrix composite as it affects dislocation motion and load transfer capability.

3.4 Discussion

The grain sizes for the S-350, S-375, and S-425 samples fall within the Hall-Petch breakdown and inversion regimes laid out by Zheng [6], making these ideal for examining the significance of using a modified Hall-Petch model to include the inverse Hall-Petch trend. This inverse trend is only possible with the transition of slip-dominated to grain boundary-mediated plasticity, and would be hindered by the presence of second-phase particles residing at grain boundaries. While this study does show these particles at grain boundaries, the low volume fractions (~1%) and large sizes of the particles (200-

260nm) limit the efficacy of these particles in pinning grain boundaries and preventing grain boundary sliding. In addition to Hall-Petch strengthening, the models for load transfer, coefficient of thermal expansion and elastic mismatch, and Orowan strengthening will be evaluated.

3.4.1 Load transfer model

The load transfer model estimates the increased strength arising from the ability of the metal-matrix composite to transfer the load from the softer matrix to the harder reinforcement phase. To properly transfer the load from the matrix to the reinforcement, a coherent interface is required. Additionally, the size and amount of reinforcement affect the extent of strengthening. Smaller particles and low volume of reinforcement do not strengthen as well as there is less reinforcement to transfer the load to. This strengthening from load transfer is typically modeled using the shear lag model or a variation of this, and the variation used for equiaxed particulate reinforcements as given by:

$$\Delta\sigma_{LT} = \frac{1}{2}\upsilon_p\sigma_m$$

In this equation, ν_p is the volume fraction of the particulate phase and σ_m is the yield strength of the matrix without reinforcement. Using an estimate of 5MPa for the yield strength of unreinforced magnesium [24], and the volume fraction values listed in Table 1, the increase in strengthening due to load transfer amounts to less than 1MPa. The low value of added strength stems mainly from the low volume fraction of the added reinforcement, where magnesium metal matrix composites typically start to exhibit significant strengthening with additions of 0.5-2 wt% for yttria reinforcements [25]–[29].

3.4.2 Coefficient of thermal expansion and elastic modulus mismatch models

The effect of thermal stresses can also cause strengthening with the creation of geometrically necessary dislocations that are required to accommodate the differences in thermal expansions between the matrix and particle reinforcement. The coefficient of thermal expansion and elastic modulus mismatch model can be represented using the Taylor equation:

$$\Delta\sigma_{CTE+EM} = \sqrt{3}\beta Gb\left(\sqrt{\rho^{CTE}} + \sqrt{\rho^{EM}}\right)$$

Where β is a constant (empirically determined to be approximately 1.25 [24]), G is the shear modulus of the matrix, b is the burger vector of the matrix, ρ^{CTE} is the dislocation density due to the contraction upon cooling associated with the difference in coefficients of thermal expansion, and ρ^{EM} is the dislocation density due to the strain induced upon cooling around the particle. The expressions for the dislocation densities are given by:

$$\rho^{CTE} = \frac{A\Delta\alpha\Delta T v_p}{b d_p\left(1 - v_p\right)}$$

$$\rho^{EM} = \frac{6v_p}{\pi {d_p}^3}\varepsilon$$

A is a constant representing the transparency of the dislocation forest for basal-basal interactions (0.2 for magnesium [24]), Δα is the difference in thermal expansion coefficients between the matrix and reinforcement, ΔT is the temperature excursion, ν_p is the volume fraction of particulates, b is the Burgers vector, d_p is the particle diameter, and ε is the plastic strain which can be calculated as ΔαΔT [30]. The strengthening in this

case arises from the number of dislocations generated during the cooling process, which is inversely dependent on the size and directly dependent on the volume fraction of the reinforcement phase. As stated previously, the volume fraction of reinforcement seen in this study is not large enough to cause significant strengthening. This coupled with the relatively large particulate diameter when compared with the significant strengthening seen in studies with yttria reinforcements sub-50nm [25], [26], [29], [31], provide a total strengthening contribution from geometrically necessary dislocations of <1MPa.

3.4.3 Orowan strengthening model

Fine particles contribute to strengthening through the Orowan mechanism, and is modeled as:

$$\Delta\sigma_{OR} = M\frac{0.4Gb}{\pi\bar{\lambda}}\frac{ln(\bar{d}/b)}{\sqrt{1-\upsilon_m}}$$

Where M is a constant representing the mean matrix orientation factor (6.5 for magnesium [24]), G is the shear modulus, b is the Burgers vector, $\bar{d}$ is the mean grain size of the matrix, $\bar{\lambda}$ is the mean inter-particle spacing, and ν_m is the Poisson's ratio of the matrix. The dominant variables affecting the degree of strengthening from this model are the mean grain size of the matrix and the mean interparticle spacing. While a larger grain size results in a stronger strengthening event for a given interparticle spacing, a smaller interparticle spacing results in greater strengthening for a given grain size. The effect of the smaller interparticle spacing, however, is more prominent than the effect of increasing the grain size, following a power trend and logarithmic trend respectively. This model estimates a strengthening contribution of 21.99MPa, 24.74MPa, and 26.7MPa for the

SPS-350, SPS-375, SPS-425 samples respectively. Interparticle spacing depends on both the size and volume fraction of the particles. While it has already been determined that the volume fraction is much less and the particle size is much larger than other studies with a similar reinforcement type in magnesium, there is still anticipated to be some degree of strengthening due to the Orowan effect. One factor that has not been addressed is the location of the particles with respect to the grain boundaries. For the full Orowan effect to take place, particles need to be located within the grains instead of at the grain boundaries, and this study shows the presence of particles in both locations, thereby the full extent of the predicted Orowan strengthening is not being realized.

3.4.4 Hall-Petch strengthening model

Lastly, we evaluate the Hall-Petch strengthening model which has been modeled by:

$$\Delta\sigma_{HP} = \sigma_0 + {}^{k}/_{\sqrt{d}}$$

Where σ_0 is the Peierls stress of the matrix, k is the empirical Hall-Petch coefficient, and d is the grain size of the matrix. Using a Hall-Petch coefficient of 260 MPa- $\mu m^{-1/2}$ the strengthening increment due to grain boundary strengthening is 244MPa for S-350, 149MPa for S-375, and 130MPa for S-425. This strengthening places Hall-Petch as the dominant strengthening mechanism over load transfer, CTE-EM mismatch, and Orowan strengthening. One consideration in magnesium is the tendency to undergo grain growth at low temperatures due to the low melting temperature leading to accelerated recovery and recrystallization activation [6], [7], [20], and therefore the temperature and the

amount of time the system is exposed to the temperature is of concern when it comes to magnesium alloys.

The SPS process uses Joule heating which shortens the time the sample is subjected to heat in comparison with heating by other methods, which in turn, limits the amount of grain growth which is dependent on both temperature and time [32]–[35]. Despite the use of SPS to limit heating time, it would still be expected for magnesium to undergo grain growth under any application of temperature unless otherwise impeded. Pure magnesium rolled sheets have been shown to undergo grain growth from 16.36μm to 21.45μm, 24.22μm, 28.5μm, and 42.84μm after 15 minutes exposure to 150°C, 200°C, 300°C, and 400°C respectively [36].

Grain growth kinetics is also affected by the amount of stored energy in the system which typically postpones the onset of grain growth. Additionally, grain growth can be impeded by through Zener pinning from second phase particles or added reinforcements causing grain boundary locking or drag depending on the location of these particles. Production of magnesium alloys through high-energy methods such as milling, can retain fine grain structure post compaction and annealing methods with a final grain size sub-100nm [37], [38]. Despite the success of retaining a nanometer-range microstructure in these studies, most of the literature found on magnesium-based metal matrix composites result in matrix grain sizes >5μm [27]–[29], [39]–[41], with the finest microstructure obtained through secondary processing such as extrusion [38], [42], [43]. The grain sizes achieved in this study are sub-5μm, which can be attributed to recovery and recrystallization of a system that was highly energized during milling, and a small

degree of grain boundary locking and drag due to the reinforcement phases residing at the grain boundaries and within the grain interior.

3.4.5 Model Summation

Typically, these strengthening effects have been taken into account using linear superposition given by:

$$\sigma_{composite} = \sigma_m + \sum_i \Delta\sigma_i$$

However, this method has consistently overpredicted the actual strength found using experimental data. Clyne et al. proposed the use of a quadratic superposition model that better accounts for the interaction of individual strengthening mechanisms with each other [44], [45], given by:

$$\sigma_{composite} = \sigma_m + \sqrt{\sum_i \Delta\sigma_i^2}$$

Using this method, the overall strengthening can be estimated as seen in Table 2. The anticipated strength taken from the summation of individual strengthening mechanisms overestimates the actual sample yield strength as calculated from the Vickers hardness results and the Tabor relation σ_{ys} = HV/3 [46], [47]. Both the linear and quadratic strengthening mechanism models have been shown to overestimate the experimental yield strength [4]. In a study on a Mg-Y alloy, Dong Qiu experimentally determined that the summation exponent can vary based on grain size, where they found an exponent of 1.5 to be ideal for their case [48]. This effect was shown to be more pronounced at larger grain sizes (~180μm), as the Hall-Petch strengthening mechanism

begins to dominate other strengthening mechanisms at smaller grain sizes (~25μm). Extrapolating from this study, as grain size decreases, the validity of the strengthening mechanism superposition models become secondary to Hall-Petch strengthening models overall.

Table 3-2 also points to the dominance of Hall-Petch strengthening over the other strengthening mechanisms, which is alignment with the sub-5μm grain size. However, there is a variety of literature showing the Hall-Petch relation starts to break down at grain sizes below 5μm in magnesium. This breakdown in magnesium has been attributed to the transition of dominant deformation modes from dislocation-mediated plasticity, upon which the Hall-Petch relation is based, to grain-boundary-mediated plasticity [6], [49]–[51]. This softening effect could account for the lower experimental strength (through Tabor's approximation) in comparison with the strengthening model prediction. Contradictory to this, the yttrium-hydride at grain boundaries would act to both retard grain growth, but also to prevent grain-boundary-mediated plasticity, thereby exhibiting additional strengthening rather than a softening effect.

Table 3-2 Summary of strengthening mechanism calculated values and comparison to the experimental Vickers hardness results, and Tabor's relation yield strength estimate.

		SPS-350 (MPa)	SPS-375 (MPa)	SPS-425 (MPa)
$\Delta\sigma_o$	Peierls Stress*	5	5	5
$\Delta\sigma_{LT}$	Load Transfer Strengthening	0.371	0.4305	0.3535
$\Delta\sigma_{CTE+EM}$	CTE and EM Mismatch Strengthening	0.05	0.09	0.07
$\Delta\sigma_{Or}$	Orowan Strengthening	21.99	24.74	26.70
$\Delta\sigma_{HP}$	Hall-Petch Strengthening**	244	149	130
σ_{MMC}	Theoretical MMC Strength	133.913	159.0165	150.4727
σ_{Tabor}	Tabor's Estimation from Experimental Hardness***	122.5	119.56	130.03

* Peierls stress taken from [24].
** A Hall-Petch coefficient of 260 MPa-$\mu m^{-1/2}$ was used for all cases following the normal Hall-Petch trend coefficient from [6].
*** Tabor's relation coefficients range from 2.3-3.7 [52]. A coefficient of 3.3 was used in these calculations in alignment with [53].

The results shown in table 3-2 represent the use of conventional Hall-Petch strengthening, which, on its own does not elucidate much other than the overestimation of the strength when compared to the Tabor's estimate. Therefore, Hall-Petch coefficients taking into account the breakdown and inversion regimes as used by Zheng [6], were applied, resulting in a calculated strengthening of 141MPa for S-350, 157MPa for S-375, and 150MPa for S-425. Fig. 5 shows a comparison of using conventional Hall-Petch modeling vs using modified Hall-Petch modeling in estimating overall strength. Fig. 3-

5A shows a large deviation at small grain sizes, with a closer fit as grain size increasing. Alternatively, by using the Hall-Petch breakdown and inversion modeling, the estimation fits closer to the experimental results even at smaller grain sizes. While not perfect, this indicates the potential of producing a model that can more closely approximate the actual strength of a magnesium-based metal matrix composite where grain boundary strengthening tends to dominate the overall strengthening of the system.

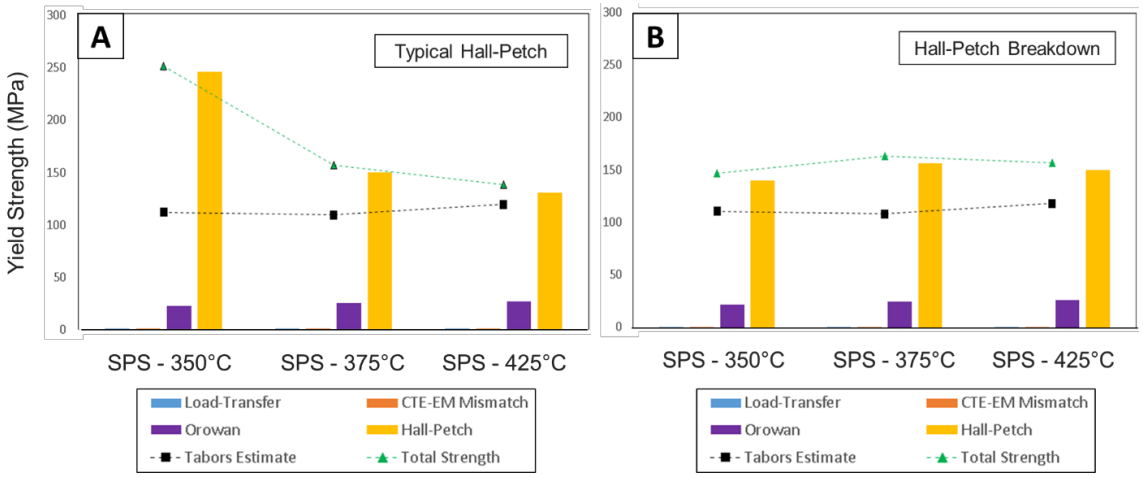

Figure 3-5 Comparison of the A) typical Hall-Petch strengthening model and B) modified Hall-Petch strengthening model including the contribution from each strengthening mechanism, the summed estimated strength, and the Tabor's estimate from experimental results.

3.4.6 Potential for variability

Closer accuracy of the strength estimate depends on how well the parameters for the Hall-Petch coefficient and Tabor's relation coefficient fit with experimental data across materials. The Hall-Petch coefficient varies widely between different magnesium alloys and the extant literature lacks a clear consensus on the Hall-Petch breakdown and inversed regimes. Most studies on magnesium report a coefficient between 250 and 280 MPa-$\mu m^{-1/2}$ [6], [54], [55] for a regime in which the Hall-Petch correlation is accurate.

Within the breakdown and inversed regimes, however, the literature is less expansive, and a much wider variation in coefficients exist, ranging from 32 to 105 MPa- $\mu m^{-1/2}$ [6], [50], [55] for the breakdown regime and from -96 to -175 MPa-$\mu m^{-1/2}$ [6], [50] in the inversed regime. This makes the selection of an appropriate Hall-Petch coefficient difficult without additional experimental data to validate the coefficient choice as the material approaches 5μm or below. Similarly, the Tabor approximation has been correlated to experimental data for coefficients between 2.3 and 3.7. Without accurate yield strength data, 3.3 for the Tabor's coefficient was used to estimate the yield strength from Vickers hardness data. This is the coefficient used by Somekawa while investigating grain boundary sliding in magnesium [53], however, it is unclear how well this coefficient will fit the system in this study as there is the possibility that some grains were pinned by YH_2 particles and were unable to slide.

Additionally, the overestimation of strength could be due to the reinforcement particle coherency and density of the samples. Figure 3-4 shows high resolution TEM showing the semi-coherency of the particles. This would lessen the amount of load that can be transferred from the matrix to the harder reinforcement before yielding at the interface. Similarly, the consolidated samples achieve >99% relative density, reaching higher densities with higher consolidation temperature. A sample that is denser would present with higher hardness as there is less porosity that can contribute to premature failure.

3.5 Conclusions

In this study, a magnesium-based metal-matrix composite with YH_2 reinforcements was used to examine the impact the inverse Hall-Petch trend can have on the current models used to estimate strength. By using the Hall-Petch coefficients for the corresponding grain sizes used by Zheng [6], it was shown that the approximated strength more closely matches the experimental hardness data, and is more pronounced at smaller grain sizes. In magnesium systems which tend toward grain-boundary strengthening as the dominant mechanism, coupled with Hall-Petch softening at relatively large grain sizes, grain-size-specific Hall-Petch coefficients should be taken into account and incorporated into the strengthening models. While there is plenty of room for variability, and the modified Hall-Petch strengthening model still overestimates the experimental results, this is a promising step toward increasing the accuracy of the current models.

References

[1] A. Bahador, J. Umeda, E. Hamzah, F. Yusof, X. Li, and K. Kondoh, "Synergistic strengthening mechanisms of copper matrix composites with TiO2 nanoparticles," *Materials Science and Engineering: A*, vol. 772, p. 138797, Jan. 2020, doi: 10.1016/j.msea.2019.138797.

[2] B. Chen *et al.*, "Length effect of carbon nanotubes on the strengthening mechanisms in metal matrix composites," *Acta Materialia*, vol. 140, pp. 317–325, Nov. 2017, doi: 10.1016/j.actamat.2017.08.048.

[3] A. Sanaty-Zadeh, "Comparison between current models for the strength of particulate-
reinforced metal matrix nanocomposites with emphasis on consideration of Hall–Petch effect," *Materials Science and Engineering: A*, vol. 531, pp. 112–118, Jan. 2012, doi: 10.1016/j.msea.2011.10.043.

[4] C.-S. Kim *et al.*, "Prediction models for the yield strength of particle-reinforced unimodal pure magnesium (Mg) metal matrix nanocomposites (MMNCs)," *J Mater Sci*, vol. 48, no. 12, pp. 4191–4204, Jun. 2013, doi: 10.1007/s10853-013-7232-x.

[5] M. A. Meyers, A. Mishra, and D. J. Benson, "Mechanical properties of nanocrystalline materials," *Progress in Materials Science*, vol. 51, no. 4, pp. 427–556, May 2006, doi: 10.1016/j.pmatsci.2005.08.003.

[6] R. Zheng, J.-P. Du, S. Gao, H. Somekawa, S. Ogata, and N. Tsuji, "Transition of dominant deformation mode in bulk polycrystalline pure Mg by ultra-grain refinement down to sub-micrometer," *Acta Materialia*, vol. 198, pp. 35–46, Oct. 2020, doi: 10.1016/j.actamat.2020.07.055.

[7] R. B. Figueiredo, S. Sabbaghianrad, A. Giwa, J. R. Greer, and T. G. Langdon, "Evidence for exceptional low temperature ductility in polycrystalline magnesium processed by severe plastic deformation," *Acta Materialia*, vol. 122, pp. 322–331, Jan. 2017, doi: 10.1016/j.actamat.2016.09.054.

[8] Z. Zeng, J.-F. Nie, S.-W. Xu, C. H. J. Davies, and N. Birbilis, "Super-formable pure magnesium at room temperature," *Nat Commun*, vol. 8, no. 1, p. 972, Oct. 2017, doi: 10.1038/s41467-017-01330-9.

[9] Y. Cheng, Z. Cui, L. Cheng, D. Gong, and W. Wang, "Effect of particle size on densification of pure magnesium during spark plasma sintering," *Advanced Powder Technology*, vol. 28, no. 4, pp. 1129–1135, Apr. 2017, doi: 10.1016/j.apt.2017.01.017.

[10] W. N. A. W. Muhammad, Z. Sajuri, Y. Mutoh, and Y. Miyashita, "Microstructure and mechanical properties of magnesium composites prepared by spark plasma sintering technology," *Journal of Alloys and Compounds*, vol. 509, no. 20, pp. 6021–6029, May 2011, doi: 10.1016/j.jallcom.2011.02.153.

[11] R. Liu, W. Wang, H. Chen, Z. Lu, W. Zhao, and T. Zhang, "Densification of pure magnesium by spark plasma sintering-discussion of sintering mechanism," *Advanced Powder Technology*, vol. 30, no. 11, pp. 2649–2658, Nov. 2019, doi: 10.1016/j.apt.2019.08.012.

[12] D. Setoyama, M. Ito, J. Matsunaga, H. Muta, M. Uno, and S. Yamanaka, "Mechanical properties of yttrium hydride," *Journal of Alloys and Compounds*, vol. 394, no. 1, pp. 207–210, May 2005, doi: 10.1016/j.jallcom.2004.10.035.

[13] F. J. Humphreys and M. G. Ardakani, "Grain boundary migration and Zener pinning in particle-containing copper crystals," *Acta Materialia*, vol. 44, no. 7, pp. 2717–2727, Jul. 1996, doi: 10.1016/1359-6454(95)00421-1.

[14] J. Zhou *et al.*, "Zener pinning by coherent particles: pinning efficiency and particle reorientation mechanisms," *Modelling Simul. Mater. Sci. Eng.*, vol. 25, no. 6, p. 065008, Jun. 2017, doi: 10.1088/1361-651X/aa6cfb.

[15] J. Liao, N. Yamamoto, and K. Nakata, "Effect of Dispersed Intermetallic Particles on Microstructural Evolution in the Friction Stir Weld of a Fine-Grained Magnesium Alloy," *Metall Mater Trans A*, vol. 40, no. 9, pp. 2212–2219, Sep. 2009, doi: 10.1007/s11661-009-9921-2.

[16] A. C. Hänzi *et al.*, "Design strategy for microalloyed ultra-ductile magnesium alloys," *Philosophical Magazine Letters*, May 2009, doi: 10.1080/09500830902960125.

[17] L.-M. Wu, W.-H. Wang, Y.-F. Hsu, and S. Trong, "Effects of homogenization treatment on recrystallization behavior and dispersoid distribution in an Al–Zn–Mg–Sc–Zr alloy," *Journal of Alloys and Compounds*, vol. 456, no. 1, pp. 163–169, May 2008, doi: 10.1016/j.jallcom.2007.02.054.

[18] C. J. Tweed, B. Ralph, and N. Hansen, "The pinning by particles of low and high angle grain boundaries during grain growth," *Acta Metallurgica*, vol. 32, no. 9, pp. 1407–1414, Sep. 1984, doi: 10.1016/0001-6160(84)90086-5.

[19] S. P. Ringer, W. B. Li, and K. E. Easterling, "On the interaction and pinning of grain boundaries by cubic shaped precipitate particles," *Acta Metallurgica*, vol. 37, no. 3, pp. 831–841, Mar. 1989, doi: 10.1016/0001-6160(89)90010-2.

[20] Q. Miao, L. Hu, X. Wang, and E. Wang, “Grain growth kinetics of a fine-grained AZ31 magnesium alloy produced by hot rolling,” *Journal of Alloys and Compounds*, vol. 493, no. 1, pp. 87–90, Mar. 2010, doi: 10.1016/j.jallcom.2009.12.049.

[21] S. Biswas, D. S. Singh, B. Beausir, L. S. Toth, and S. Suwas, “Thermal Response on the Microstructure and Texture of ECAP and Cold-Rolled Pure Magnesium,” *Metall and Mat Trans A*, vol. 46, no. 6, pp. 2598–2613, Jun. 2015, doi: 10.1007/s11661-015-2846-z.

[22] H. Y. Chao, H. F. Sun, W. Z. Chen, and E. D. Wang, “Static recrystallization kinetics of a heavily cold drawn AZ31 magnesium alloy under annealing treatment,” *Materials Characterization*, vol. 62, no. 3, pp. 312–320, Mar. 2011, doi: 10.1016/j.matchar.2011.01.007.

[23] C. W. Su, L. Lu, and M. O. Lai, “Recrystallization and grain growth of deformed magnesium alloy,” *Philosophical Magazine*, vol. 88, no. 2, pp. 181–200, Jan. 2008, doi: 10.1080/14786430701805566.

[24] B. Q. Han and D. C. Dunand, “Microstructure and mechanical properties of magnesium containing high volume fractions of yttria dispersoids,” *Materials Science and Engineering: A*, vol. 277, no. 1, pp. 297–304, Jan. 2000, doi: 10.1016/S0921-5093(99)00074-X.

[25] C. S. Goh, J. Wei, L. C. Lee, and M. Gupta, “Properties and deformation behaviour of Mg–Y2O3 nanocomposites,” *Acta Materialia*, vol. 55, no. 15, pp. 5115–5121, Sep. 2007, doi: 10.1016/j.actamat.2007.05.032.

[26] S. F. Hassan, “Effect of primary processing techniques on the microstructure and mechanical properties of nano-Y2O3 reinforced magnesium nanocomposites,” *Materials Science and Engineering: A*, vol. 528, no. 16, pp. 5484–5490, Jun. 2011, doi: 10.1016/j.msea.2011.03.063.

[27] S. F. Hassan, K. S. Tun, and M. Gupta, “Effect of sintering techniques on the microstructure and tensile properties of nano-yttria particulates reinforced magnesium nanocomposites,” *Journal of Alloys and Compounds*, vol. 509, no. 11, pp. 4341–4347, Mar. 2011, doi: 10.1016/j.jallcom.2011.01.064.

[28] K. S. Tun and M. Gupta, “Improving mechanical properties of magnesium using nano-yttria reinforcement and microwave assisted powder metallurgy method,” *Composites Science and Technology*, vol. 67, no. 13, pp. 2657–2664, Oct. 2007, doi: 10.1016/j.compscitech.2007.03.006.

[29] S. F. Hassan and M. Gupta, “Development of nano-Y2O3 containing magnesium nanocomposites using solidification processing,” *Journal of Alloys and Compounds*, vol. 429, no. 1, pp. 176–183, Feb. 2007, doi: 10.1016/j.jallcom.2006.04.033.

[30] R. Raj and D. Thakur, “Effect of particle size and volume fraction on the strengthening mechanisms of boron carbide reinforced aluminum metal matrix composites,” *Proceedings of the Institution of Mechanical Engineers, Part C: Journal of Mechanical Engineering Science*, vol. 233, no. 4, pp. 1345–1356, Feb. 2019, doi: 10.1177/0954406218771997.

[31] K. S. Tun and M. Gupta, “Effect of extrusion ratio on microstructure and mechanical properties of microwave-sintered magnesium and Mg/Y2O3 nanocomposite,” *J Mater Sci*, vol. 43, no. 13, pp. 4503–4511, Jul. 2008, doi: 10.1007/s10853-008-2649-3.

[32] G. T. Higgins, “Grain-Boundary Migration and Grain Growth,” *Metal Science*, vol. 8, no. 1, pp. 143–150, Jan. 1974, doi: 10.1179/msc.1974.8.1.143.

[33] R. Orrù, R. Licheri, A. M. Locci, A. Cincotti, and G. Cao, “Consolidation/synthesis of materials by electric current activated/assisted sintering,” *Materials Science and Engineering: R: Reports*, vol. 63, no. 4, pp. 127–287, Feb. 2009, doi: 10.1016/j.mser.2008.09.003.

[34] O. Guillon *et al.*, “Field-Assisted Sintering Technology/Spark Plasma Sintering: Mechanisms, Materials, and Technology Developments,” *Advanced Engineering Materials*, vol. 16, no. 7, pp. 830–849, 2014, doi: 10.1002/adem.201300409.

[35] A. V. Ragulya, “Fundamentals of Spark Plasma Sintering,” in *Encyclopedia of Materials: Science and Technology*, K. H. J. Buschow, R. W. Cahn, M. C. Flemings, B. Ilschner, E. J. Kramer, S. Mahajan, and P. Veyssière, Eds. Oxford: Elsevier, 2010, pp. 1–5. doi: 10.1016/B978-008043152-9.02249-1.

[36] D. Panda, R. K. Sabat, S. Suwas, V. D. Hiwarkar, and S. K. Sahoo, “Texture weakening in pure magnesium during grain growth,” *Philosophical Magazine*, vol. 99, no. 11, pp. 1362–1385, Jun. 2019, doi: 10.1080/14786435.2019.1581382.

[37] P. Cao, L. Lu, and M. O. Lai, “Grain growth and kinetics for nanocrystalline magnesium alloy produced by mechanical alloying,” *Materials Research Bulletin*, vol. 36, no. 5, pp. 981–988, Mar. 2001, doi: 10.1016/S0025-5408(01)00578-5.

[38] H. Yi *et al.*, “Fabrication of a bulk GdN nanoparticles-reinforced Mg-Gd matrix nanocomposite with phenomenal mechanical properties,” *Materials Letters*, vol. 185, pp. 127–130, Dec. 2016, doi: 10.1016/j.matlet.2016.08.123.

[39] S. F. Hassan and M. Gupta, “Development of high performance magnesium nano-composites using nano-Al2O3 as reinforcement,” *Materials Science and Engineering: A*, vol. 392, no. 1, pp. 163–168, Feb. 2005, doi: 10.1016/j.msea.2004.09.047.

[40] B. W. Chua, L. Lu, and M. O. Lai, “Influence of SiC particles on mechanical properties of Mg based composite,” *Composite Structures*, vol. 47, no. 1, pp. 595–601, Dec. 1999, doi: 10.1016/S0263-8223(00)00031-3.

[41] S. Xiang, X. Wang, M. Gupta, K. Wu, X. Hu, and M. Zheng, “Graphene nanoplatelets induced heterogeneous bimodal structural magnesium matrix composites with enhanced mechanical properties,” *Sci Rep*, vol. 6, no. 1, p. 38824, Dec. 2016, doi: 10.1038/srep38824.

[42] L. Zhang *et al.*, “Microstructure and mechanical properties of the carbon nanotubes
reinforced AZ91D magnesium matrix composites processed by cyclic extrusion and compression,” *Materials Science and Engineering: A*, vol. 689, pp. 427–434, Mar. 2017, doi: 10.1016/j.msea.2017.02.076.

[43] Y. Chen, S. Tekumalla, Y. B. Guo, and M. Gupta, “Introducing Mg-4Zn-3Gd-1Ca/ZnO nanocomposite with compressive strengths matching/exceeding that of mild steel,” *Sci Rep*, vol. 6, no. 1, p. 32395, Aug. 2016, doi: 10.1038/srep32395.

[44] R. Casati and M. Vedani, “Metal Matrix Composites Reinforced by Nano-Particles—A Review,” *Metals*, vol. 4, no. 1, Art. no. 1, Mar. 2014, doi: 10.3390/met4010065.

[45] M. Malaki *et al.*, “Advanced Metal Matrix Nanocomposites,” *Metals*, vol. 9, no. 3, Art. no. 3, Mar. 2019, doi: 10.3390/met9030330.

[46] D. Tabor, “The physical meaning of indentation and scratch hardness,” *Br. J. Appl. Phys.*, vol. 7, no. 5, pp. 159–166, May 1956, doi: 10.1088/0508-3443/7/5/301.

[47] J. R. Cahoon, W. H. Broughton, and A. R. Kutzak, “The determination of yield strength from hardness measurements,” *Metall Mater Trans B*, vol. 2, no. 7, pp. 1979–1983, Jul. 1971, doi: 10.1007/BF02913433.

[48] D. Qiu and M.-X. Zhang, “Strengthening Mechanisms and their Superposition Law in an Age-Hardenable Mg-10 wt pct Y Alloy,” *Metall Mater Trans A*, vol. 43, no. 9, pp. 3314–3324, Sep. 2012, doi: 10.1007/s11661-012-1162-0.

[49] H. J. Choi, Y. Kim, J. H. Shin, and D. H. Bae, “Deformation behavior of magnesium in the grain size spectrum from nano- to micrometer,” *Materials Science and*

Engineering: A, vol. 527, no. 6, pp. 1565–1570, Mar. 2010, doi: 10.1016/j.msea.2009.10.035.

[50] M. M. Castro, P. H. R. Pereira, A. Isaac, T. G. Langdon, and R. B. Figueiredo, "Inverse Hall–Petch Behaviour in an AZ91 Alloy and in an AZ91–Al2O3 Composite Consolidated by High-Pressure Torsion," *Advanced Engineering Materials*, vol. 22, no. 10, p. 1900894, 2020, doi: 10.1002/adem.201900894.

[51] Z. C. Cordero, B. E. Knight, and C. A. Schuh, "Six decades of the Hall–Petch effect – a survey of grain-size strengthening studies on pure metals," *International Materials Reviews*, vol. 61, no. 8, pp. 495–512, Nov. 2016, doi: 10.1080/09506608.2016.1191808.

[52] S. N. Naik and S. M. Walley, "The Hall–Petch and inverse Hall–Petch relations and the hardness of nanocrystalline metals," *J Mater Sci*, vol. 55, no. 7, pp. 2661–2681, Mar. 2020, doi: 10.1007/s10853-019-04160-w.

[53] H. Somekawa and T. Mukai, "Effect of grain boundary structures on grain boundary sliding in magnesium," *Materials Letters*, vol. 76, pp. 32–35, Jun. 2012, doi: 10.1016/j.matlet.2012.02.010.

[54] C. H. Caceres, G. E. Mann, and J. R. Griffiths, "Grain Size Hardening in Mg and Mg-Zn Solid Solutions," *Metall Mater Trans A*, vol. 42, no. 7, pp. 1950–1959, Jul. 2011, doi: 10.1007/s11661-010-0599-2.

[55] H. Somekawa and T. Mukai, "Hall–Petch Breakdown in Fine-Grained Pure Magnesium at Low Strain Rates," *Metall and Mat Trans A*, vol. 46, no. 2, pp. 894–902, Feb. 2015, doi: 10.1007/s11661-014-2641-2.

Chapter 4 - Improved hardness and thermal stability in a Mg-Li-Ca alloy processed by high pressure torsion

H.K. Salvador[1], S.N. Mathaudhu[1]

[1]University of California, Riverside

Abstract

Magnesium-lithium alloys present a class of super-light alloys, however, suffer from poor thermal stability and poor bulk strength. Grain refinement is effective in strengthening these alloys, however, this adds to the poor thermal stability. This limits the potential uses for structural Mg-Li if improvements in strength are unable to subsist when subject to heat. In this study, a Mg-3.53Li-0.61Ca (wt%) alloy was processed by high pressure torsion (HPT) to achieve a sub-micron grain size improving the hardness of the alloy to the high end of what is seen in magnesium alloys as a whole and among the highest seen in Mg-Li alloys to date. This Mg-Li alloy also retained the improved hardness up to annealing temperatures of 150°C, a marked improvement over room temperature and low temperature instability of the alloy system. Both the hardness and the stability can be attributed to grain refinement with stabilization via second-phase particles providing Zener pinning and precipitate strengthening. By comparing the hardness Hall-Petch trend of this study with deformed AZ31, LZ91, and Mg it was found that this study has a similar hardness trend to AZ31 and improved over that of LZ91 and Mg. This provides promise for developing stronger Mg-Li alloys that exhibit superior thermal stability over other Mg-Li alloys to date.

4.1 Introduction

Magnesium alloys have long been attractive for use in the aerospace and automotive industries for weight-loss capabilities when replacing heavier materials such as aluminum or steel. Alloying magnesium with lithium further reduces magnesium alloy densities, increasing the weight-saving potential of using this class of alloys, however, these alloys tend to exhibit lower ultimate tensile strengths, UTS, (110-200MPa [1]–[3]) and hardness (40-60HV [1], [2], [4]) than other commonly used magnesium alloys (250-365MPa and 85-100HV for WE43, AZ31B, and ZK60A [5]–[7]). Severe plastic deformation methods have had success in strengthening up to 80HV [8]–[22] and 265MPa UTS [8], [12], [15]–[18], [20] via grain refinement, however, the research focus on fine-grained Mg-Li alloys leans toward superplasticity rather than strengthening [8], [9], [17], [21], [23]–[25].

Grain refinement increases the interfacial energy of the system, providing a driving force for grain growth, causing many nano-scaled and ultra-fine-grained materials to lose their refinement, and thus mechanical properties, over time and/or when subject to temperature. Since research focus in Mg-Li is often on the superplastic behavior of the material, the ability of the material to retain the processed nanostructure is typically not addressed. Of the few studies found, Guo studied Mg-7.8Li-08Zn processed by extrusion and rolling and subsequently to annealed at temperatures from 150°C to 350°C for 1 hour [26], causing a drop in both the yield stress and ultimate tensile strength at annealing temperatures as low as 150°C due to achieving full recrystallization and grain growth. Yang investigated cold-rolled LZ91 when annealed for 1 hour at temperatures from 75°C

to 300°C [18], also demonstrating a decrease in ultimate yield stress with the lowest annealing temperature, attributed to recovery and recrystallization. Considering Mg-Li alloys exhibiting poor strength, and lose mechanical properties achieved by grain refinement at such low temperatures, the applications for these materials remains limited. Beyond grain refinement, precipitation hardening has been shown to improve the mechanical properties of Mg-Li alloys to upwards of 100HV and 350MPa UTS [27], [28], and precipitates have shown the added benefit of stabilizing grain boundaries [29]–[31]. Mg2Ca intermetallic readily forms in Mg-Li-Ca alloys and can be refined and dispersed upon processing. Nene used hot rolling to refine the LC41 grain structure to 5μm, resulting in a hardness of 67HV [20]. This particular study had a microstructure much larger than the nanometer-level grain sizes mentioned earlier, however, the hardness level is still comparable due to the fine Mg2Ca intermetallic phase in conjunction with the grain boundary strengthening. The combination of grain refinement and dispersion hardening with grain boundary pinning, has the capability to circumvent the low strength and thermal stability of Mg-Li alloys, and is a category which has not been fully explored in hexagonal Mg-Li.

In this study, the potential of the Mg-3.5Li-0.6Ca alloy to achieve and retain high hardness was analyzed and compared with literature reports on other magnesium alloys. By using HPT, the alloy was strengthened using a combination of grain refinement, dispersion hardening, and grain boundary pinning, reaching hardness above 90Hv, surpassing most hardness levels reported on magnesium-lithium alloys and comparable to some AZ31 alloys. Further, the alloy exhibited exceptional thermal stability up to 150°C,

much improved over the room temperature and low temperatures at which other Mg-Li systems have exhibited grain growth.

4.2 Methods and Materials

4.2.1 Starting Materials

The cast material for this study was provided by Terves Inc., and sent to Laboratory Testing Inc. to verify composition using inductively coupled plasma analysis in accordance with MAS-ICP Rev. 25. This testing reported the samples to consist of 3.5% lithium, 0.6% calcium and 0.002% silicon with the balance of magnesium by weight.

To relieve any residual stress from the casting process, and induce a homogenized microstructure, the cast material was heat treated in a tube furnace at 350°C under argon for 24 hours and then quenched in water. This homogenizing treatment also worked to provide a more homogenous microstructure prior to processing.

4.2.2 Severe Plastic Deformation Processing

To prepare samples for high pressure torsion processing (HPT), a diamond saw was used to cut 0.1mm thick slices from the cast bar, and a bench punch was used to punch 10mm diameter disks from those slices. These 10mm by 0.1mm disks were processed using HPT using the following pressures and anvil turns; 4GPa for ½ turn, 4GPa for 2 turns, 4GPa for 4 turns, 1GPa for 4 turns, and 5GPa for 4 turns. These conditions allow for a study including a variation of processing pressure as well as the number of turns, or total strain imposed in the material.

4.2.3 Isochronal Annealing

To evaluate the microstructural and mechanical stability of the HPT-processed material, isochronal annealing was conducted on the HPT disks processed at 1GPa for 4 turns, 4GPa for ½ turn, 2 turns, and 4 turns, and 5GPa for 4 turns. The HPT disks were sectioned into 6 equal pie pieces using a diamond saw. This pie piece geometry was used to include the full range of strain variation that exists in HPT disks, as the outer edges are subject to more strain than the center of the disk. Four pieces from each condition were used for the annealing treatments and the remaining two pieces were set aside representing the HPT condition without annealing.

Each piece for the annealing study was wrapped in steel foil and sealed within borosilicate ampules under high purity (99.99%) argon. A sealed piece within an ampule from each HPT condition was annealed in a tube furnace at 100°C, 150°C, 200°C, and 250°C for 30 minutes, using a heating ramp rate of 5°C/minute, and then quenched by breaking the ampules under water to halt the annealing process.

4.2.4 Sample preparation and characterization

As cast, homogenized, HPT, and annealed samples were prepared for characterization by mounting in acrylic and grinding the surface to 1200-grit using silicon carbide sand paper. Polishing was performed using 6μm and 1μm Advanced Abrasives Aqua-pol diamond suspension on Allied High Tech Products DiaMat polishing cloth, rinsing with soapy water, DI water, and ethanol between steps. Final polish was performed using 0.05μm water-free colloidal silica on a Final A polishing cloth (both purchased from Allied High Tech Products), rinsing with DI and ethanol after polish.

Hardness measurements were used to characterize the mechanical behavior of the material at varying conditions throughout the study. All measurements were taken using a Phase II Vickers microhardness tester at a load of 50g for 15seconds. To account for the strain variation across the HPT disk, hardness measurements were taken across the diameter of the disk with at least four lines of measurements per sample, and reported as an average with standard deviation as an indication of the variation across the disk.

X-ray diffraction (PANalytical Empyrean series 2) was performed to identify phases present and any phase transition after HPT. Phase presence was further confirmed using electron dispersive spectroscopy (ThermoFisher Scientific NNS450 SEM). Grain size of the as cast and homogenized samples were evaluated using backscatter detection electron microscopy (ThermoFisher Scientific NNS450 SEM) and lineal intercept methodology. The grain size of the samples processed by HPT were too small to resolve in SEM, leading to evaluating 4GPa-2turn and 4GPa-4turn samples using focused ion beam polished foils with transmission electron microscopy (ThermoFisher Scientific TalosL120C).

4.3 Results and Discussion

4.3.1 Grain refinement and precipitate distribution

XRD analysis shows that the as cast alloy consists of hcp-Mg with lithium in solution and Mg2Ca phases (Fig. 4-1). After homogenization at 350°C for 24 hours, and subsequent processing by high pressure torsion, the presence of the Mg2Ca intermetallic peaks remain. Beyond this, it is difficult to determine whether or not peaks fully disappear which would indicate dissolution of the precipitate into the matrix as the

Mg2Ca peaks are only marginally larger than the machine noise. Given the maximum solid solubility of calcium in magnesium is 1.34wt% at 520°C, and the starting alloy contains 0.61wt% Ca, it is possible that the homogenizing treatment temperature allowed for diffusion of Ca into the matrix, but this is unconfirmed from the present data. Similarly, there do not appear to be significant peak variations with HPT, although the small peaks make it difficult to know if HPT participates in dissolving any Ca from the intermetallic into the Mg matrix from the XRD.

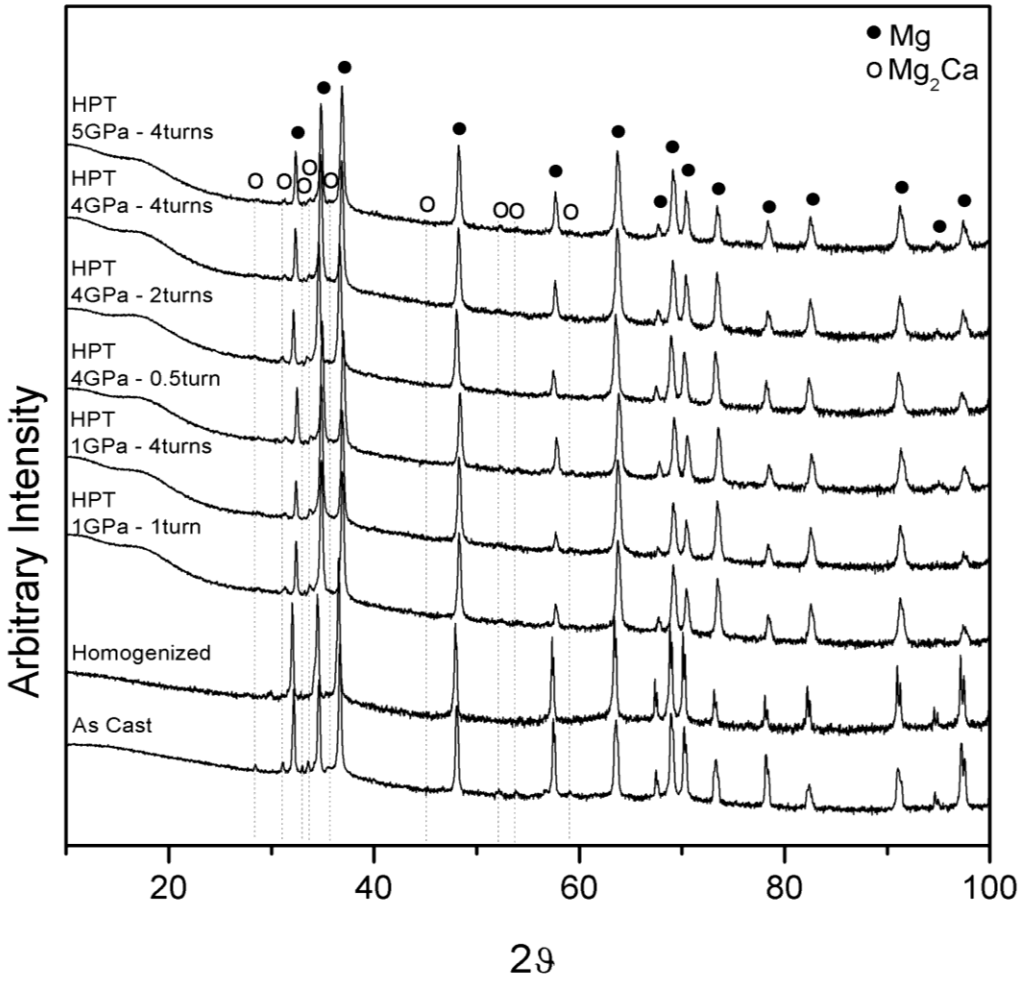

Figure 4-1 X-ray diffraction for the as cast, homogenized, and HPT conditions with Mg and Mg2Ca peaks identified.

Fig. 4-2 shows large, dendritic-like intermetallic structures are sustained from the as cast sample to the homogenized sample and throughout all HPT conditions. Analysis of smaller precipitate dispersion and location relative to the grains after HPT was difficult to discern using SEM due to the quick formation of an oxide layer.

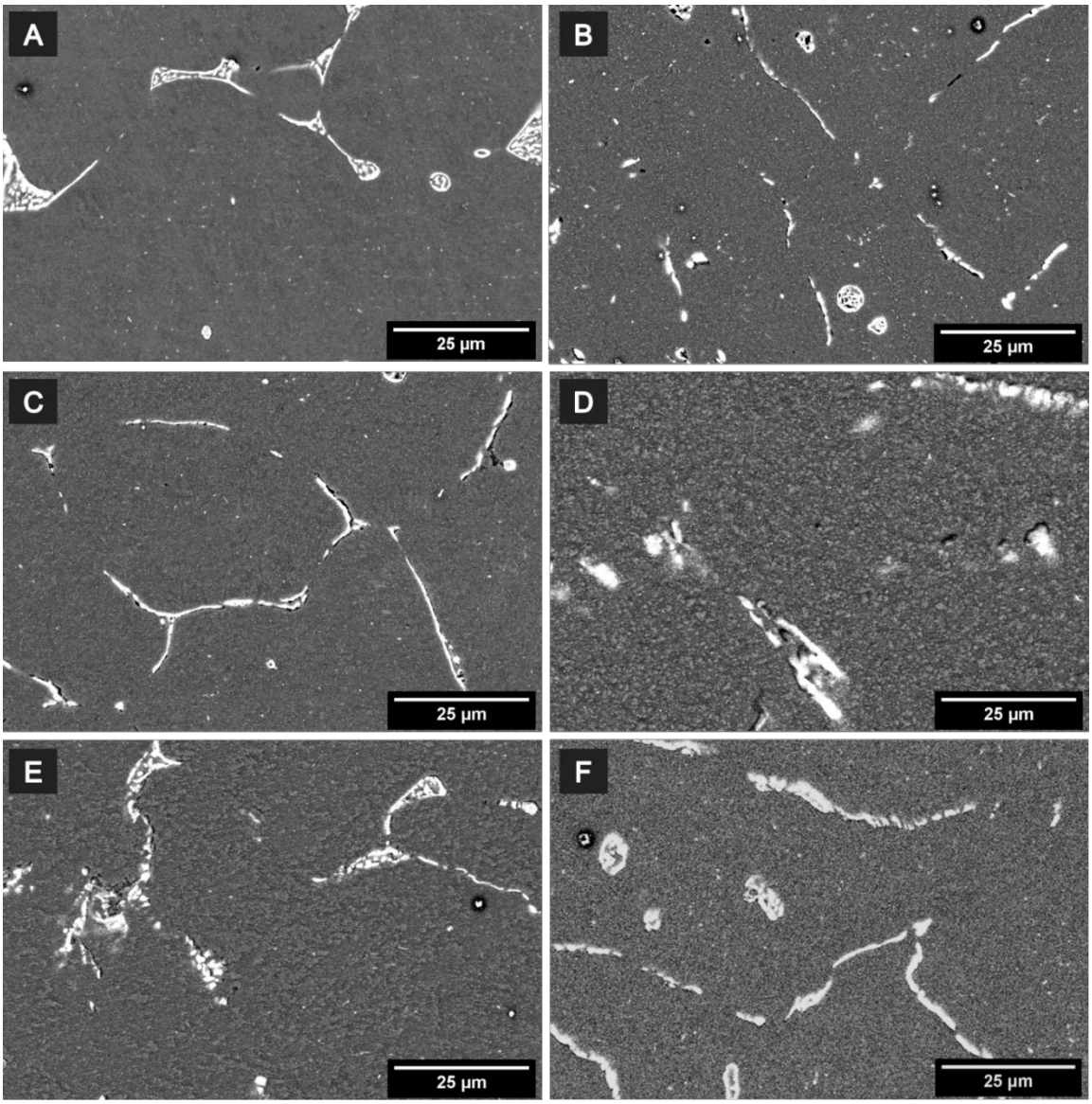

Figure 4-2 Scanning electron micrographs using backscatter electron detection for sample conditions A) homogenized, B) HPT at 4GPa for 0.5 turns, C) HPT at 4GPa for 2 turns, D) HPT at 4GPa for 4 turns, E) HPT at 1GPa for 4 turns, and F) HPT at 5GPa for 4 turns.

TEM imaging of the 4GPa-2turn and 4GPa-4turn HPT samples showing the grain size is reduced from 74.23µm in the homogenized condition to 409nm and 172nm for the 2turn and 4turn samples respectively. HPT has been used on Mg-Li base alloys to refine grains to similar sizes, although the main focus of those studies has been to use the

refined grain size to enhance ductility through grain boundary sliding [8], [9], [32], [33], whereas this study is focused on strengthening via grain refinement. As has been shown in other studies, severe plastic deformation contributes to grain refinement via dynamic recrystallization [34]–[36] and also precipitate fragmentation [37]–[39] and dispersion [39], [40], both of which are believed to have occurred in this study.

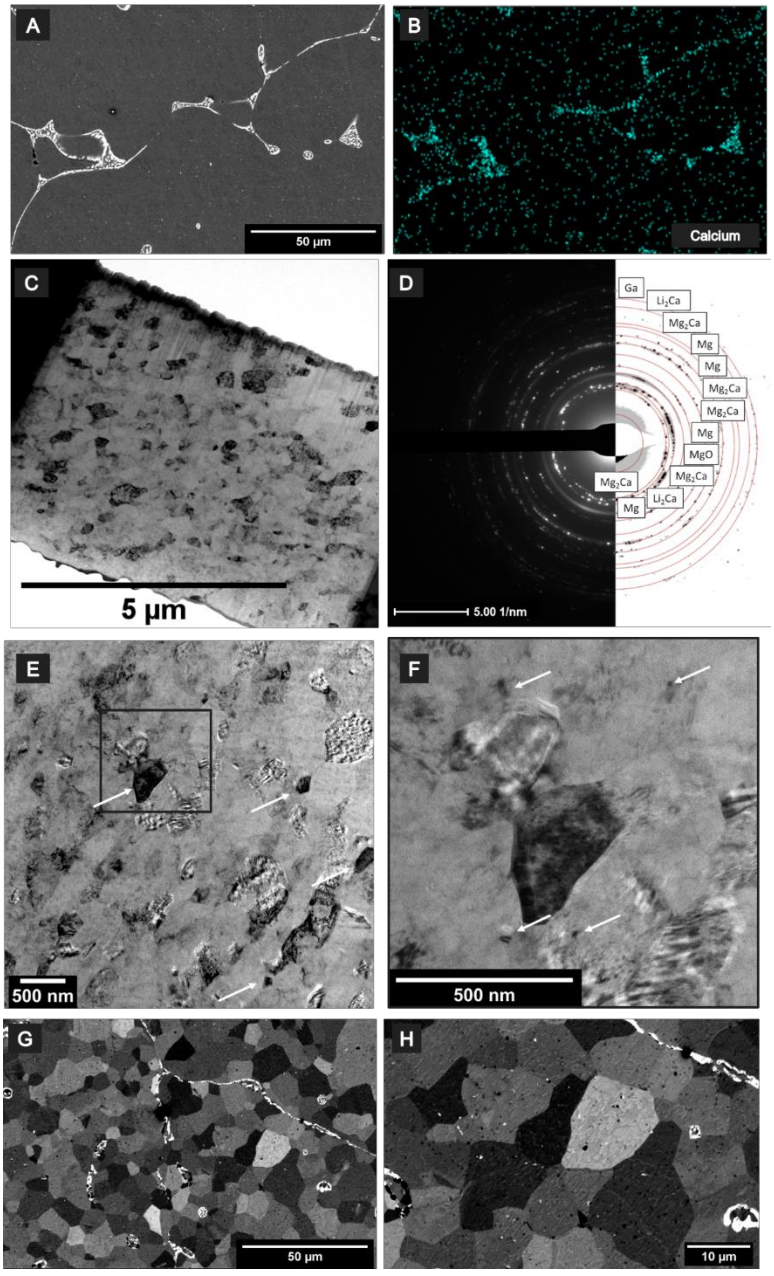

Figure 4-3 Micrographs displaying precipitate distribution in A) the homogenized state, B) the corresponding energy dispersive spectroscopy scan for calcium showing the precipitates in A are calcium-rich, C) Bright field TEM of the 4GPa-4turn sample and D) corresponding SAED with rings indexed, E) Bright field TEM of the 4GPa-2turn sample showing larger precipitates with arrows, and F) zoomed in box from image E with arrows showing smaller-scale precipitates, G) the 4GPa-2turn sample annealed at 250C for 30 minutes and H) higher magnification of image C showing the location of the small, white precipitates relative to the grains.

Additionally, while the larger precipitate networks are present in all HPT conditions, smaller-scale precipitates can be seen distributed throughout the TEM images, and the presence of Mg_2Ca is confirmed using selected area diffraction ring indexing. The smaller-scale precipitates appear to fall into two size categories: precipitates on the same scale as the magnesium grains as shown in Fig. 4-3E, and even smaller precipitates distributed throughout as shown in Fig. 4-3F. It should be noted that the assumption that contrast was used to identify the precipitates with the knowledge that Mg_2Ca is present from SAED of the full foil (Fig. 4-3D), and was not verified specifically with SAED or STEM at this time. The precipitates are assumed to have been fragmented and dispersed during HPT, however, another mechanism that could be responsible for the small-scale precipitates is through dissolution and reprecipitation when subject to pressure. This mechanism has been shown in magnesium and aluminum alloys subject to HPT where the imposed strain drives precipitate fragmentation via dislocation cutting and dissolution via atomic migration along said dislocations [41]–[43], and would explain the presence of the smallest scale precipitates.

Table 4-1 Grain size and hardness for initial conditions, HPT conditions, and select annealed conditions.

Condition	Grain Size (μm)	Hardness (HV)
As Cast	90.45	49.37 ± 2.03
Homogenized	74.23	39.82 ± 1.75
4GPa – 0.5turn	--	77.1 ±12.05
4GPa – 2turn	0.409 ± 0.079	74.66 ± 10.19
4GPa – 4turn	0.172 ± 0.045	91.54 ± 7.13
1GPa – 4turn	--	77.71 ± 8.97
5GPa – 4turn	--	92.09 ± 8.68
4GPa – 2turn (250°C anneal)	9 ± 1.12	48.57 ± 4.2
4GPa – 4turn (250°C anneal)	3.5 ± 0.42	51.15 ± 3.49

4.3.2 Discussion on hardness

Hardness results of the HPT samples show an increase over the as cast and homogenized samples, with a peak hardness of 92HV for the 5GPa-4turn sample, and is attributed to the combination of sub-micrometer grain sizes and precipitate strengthening. This study exhibits a hardness level on the high end of what is typically seen in magnesium alloys and exceeds most Mg-Li alloys with the exception of select Mg-Li-Al precipitate-strengthened alloys [27], [28], [44]. To assess the hardening capacity, hardness was plotted against the inverse square root of the grain size and fit linearly following the Hall-Petch relation, only substituting yield strength for hardness.

$$HV = HV_0 + {}^{k}/_{\sqrt{d}}$$

This capacity was plotted against plastically deformed AZ31, Mg, and LZ91 to demonstrate performance in context of other magnesium systems. The y-intercept value, HV_0, is indicative of the Peierls stress or lattice friction without the influence of grain boundary strengthening, and the slope of this plot, k, represents the hardenability of the material, with a larger slope indicating a stronger relationship between hardening and grain size.

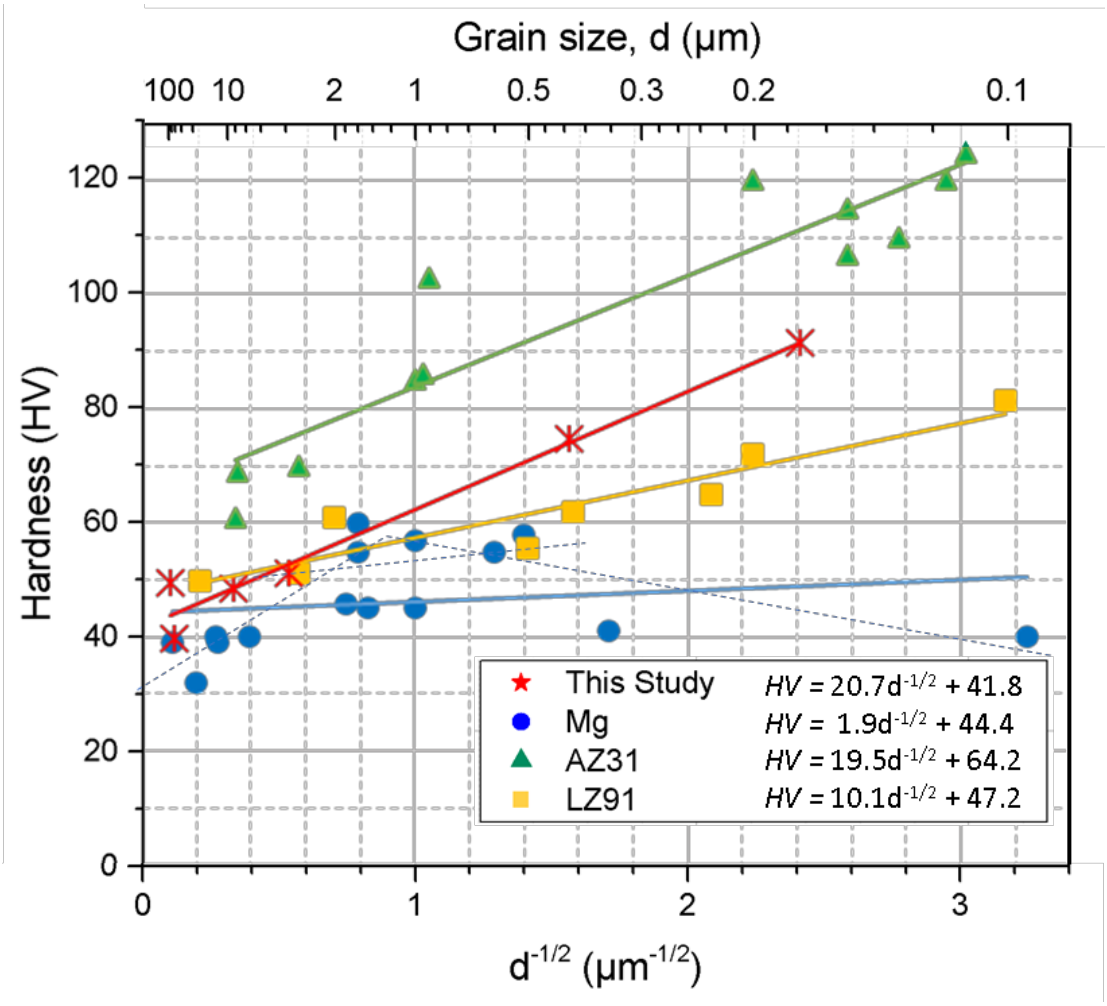

Figure 4-4 Hall-Petch relation plotted as hardness vs inverse square root of the grain size for commercially pure magnesium [45]–[56], AZ31 [46], [51], [57]–[65], and LZ91 [9], [12], [17]–[19] alloys processed by severe plastic deformation in comparison with the values found in this study.

4.3.2.1 The Hall-Petch intercept, σ_0

Without the consideration of grain boundary strengthening, HV_0 depends mainly on any added strengthening from solute additions. Since the addition of aluminum and zinc have greater solid solution strengthening ability than Li, the higher HV_0 of AZ31 over Mg and LZ91 is predicted [24], [66], [67]. LZ91 and Mg-Li-Ca are both Mg-Li base alloys and having similar HV_0 is expected, however, the solute additions should improve

the HV_0 values over unalloyed magnesium. To explain this, we need to consider the inverse Hall-Petch trend where the linear strengthening trend breaks down and inverts beyond a critical grain size and has been observed in magnesium alloys within the grain sizes plotted in Fig. 4 [68]–[72]. To account for this, dotted linear fitted lines are drawn on Fig. 4 to represent a fit for a classic Hall-Petch regime, a breakdown regime, and an inverse regime. From this, the regular Hall-Petch trend line shows a lower HV_0 as expected in comparison to alloyed magnesium.

4.3.2.2 The Hall-Petch slope, k

When assessing the response of mechanical properties to severe plastic deformation, the more interesting parameter to consider is the Hall-Petch slope. The Hall-Petch equation was developed empirically from experimental data, and there has been research suggesting other models that more closely follow the physical response of the system. Regardless of the model used, in simplistic terms, the Hall-Petch coefficient can be physically interpreted as the ability of the material to resist dislocation transmission under applied stress [73]–[75].

From Fig. 4 this study demonstrates a similar hardenability to AZ31, double that of LZ91, and about ten times larger than magnesium. It is anticipated that AZ31 will have a greater hall-Petch slope than Mg-Li alloy and Mg due to the greater effect aluminum and zinc have on increasing the critical resolved shear stress of slip systems within magnesium over lithium or without additions [76], [77]. What is unexpected is that the Mg-Li-Ca alloy in this study exhibits a hardening capacity equal to AZ31, especially as both Li and Ca have been shown to have an effect on the critical resolved shear stress and

stacking fault energy of magnesium [76], [78], [79] leading to a reduced work hardening ability compared to AZ31.

The improved hardenability stems from the second-phase particles causing both Zener pinning and grain boundary drag. The effect of precipitates and second phase particles has been shown to impact the Hall-Petch constant by effectively reducing the mean free path for dislocation motion [80]–[83]. Beyond the evidence presented in this report, the Hall-Petch constant can be affected by other factors such as the anisotropy of the system which leads into texture development, the strain rate at which the material is tested, and the grain boundary character such as high or low-angled [84]. All of these play a role in the final strengthening characteristic of the material, however, were not addressed in this study.

4.3.3 Effect of annealing temperature

The isochronal annealing study shows that the 1GPa-4turn, 4GPa-0.5turn, and 4GPa-2turn samples exhibited hardness stability up to 150°C, while the 4GPa-4turn and 5GPa-4turn samples started decreasing in hardness at 100°C. Grain size analysis of the 4GPa-2turn and 4GPa-4turn samples after annealing at 250°C for 30 minutes show that the grain sizes increased from 409nm to 9μm and 172nm to 3.5μm respectively. This demonstrates superior thermal stability to Mg-Li alloys which display low thermal stability due to the high mobility of lithium. Cold-rolled LZ91 exhibited a decrease in hardness after annealing at temperatures as low as 75°C [18] and rolled LAZ1110 underwent age softening at room temperature [85].

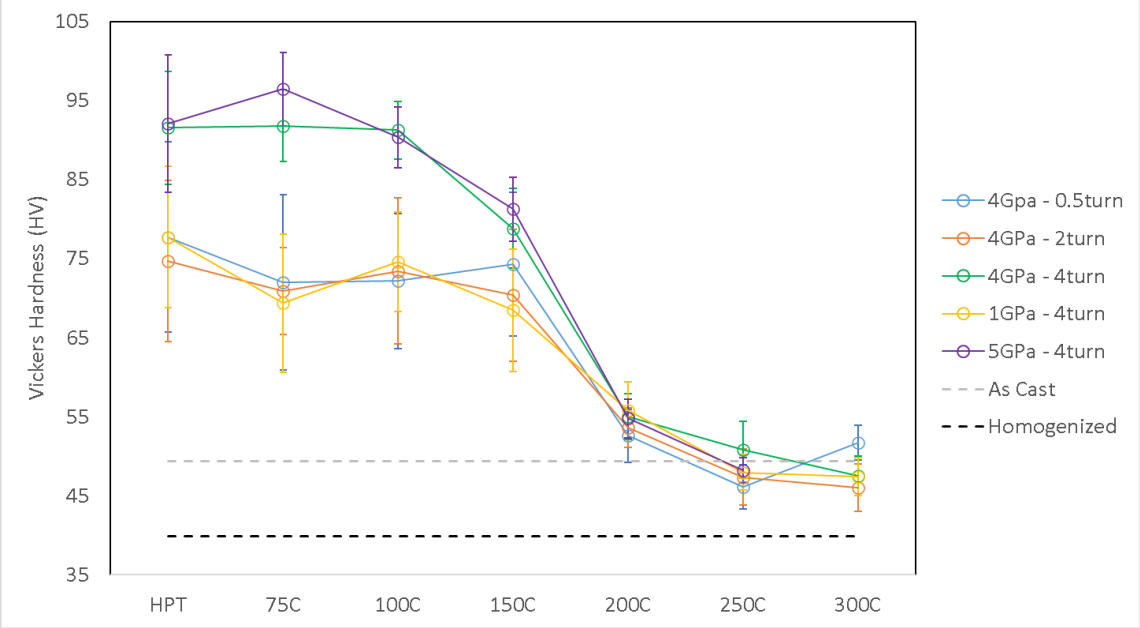

Figure 4-5 Hardness for as HPT conditions and annealing conditions.

The small precipitates shown in Fig. 4-3 are the most likely mechanism explaining the retention of fine grains due to precipitates along or nucleated at grain boundaries causing Zener pinning or residing within grains contributing to drag. In Fig. 4-3H many of the small precipitates are shown to be located within the grain interior after annealing indicating the grain boundary has broken free from the pinning effect, however, there are a few precipitates still residing at grain boundaries which is congruent with the theory that the refined precipitates maintain a pinning force even after hardness stability has been reached.

4.4 Conclusions

In summary, a Mg-3.53Li-0.61Ca (wt%) alloy was processed by high pressure torsion, followed by hardness measurements, and isochronal annealing. The following was found:

- The processing resulted in submicron refined grains along with fragmentation and dispersion of the Mg_2Ca intermetallic precipitate.
- The grain refinement contributed to Hall-Petch strengthening while the dispersed, fine intermetallic phases contributed to precipitation hardening of the HPT-processed material.
- The precipitates also acted to retard grain growth via Zener pinning. This allowed the HPT samples to retain hardness up to 150°C in the annealing treatments. Even after hardness stability is reached, the stabilized microstructure after 250°C annealing exhibit a grain size of 9μm and 3.5μm for the 4GPa-2turn and 4GPa-4turn samples respectively.
- A Hall-Petch relation was determined using the best fit linear line between points plotted on a hardness vs inverse square root of the grain size graph. The hardenability term, k, was found to be similar to that found in AZ31 alloys showing a similar hardenability capacity, whereas it was increased over that of LZ91 alloys and unalloyed magnesium due to the presence of second-phase particles.

By using HPT, a lightweight magnesium alloy was strengthened to levels among the high end of what is currently seen in magnesium alloys due to grain refinement and precipitation hardening. Further, the precipitates act to pin grain boundaries providing greater thermal stability than seen in other Mg-Li alloys. This shows promise for increasing the strength and stability capabilities of lightweight magnesium alloys. In conjunction with strengthening capability, an avenue for future work includes variation in

production and processing parameters to better control precipitate dispersion and size, aiming for only a fraction of grains pinned, allowing for plasticity by grain boundary sliding in unpinned grains. This is yet to be explored, but could prove to be a useful mechanism for circumventing the classical strength-ductility paradox.

References

[1] A. Sanschagrin, R. Tremblay, R. Angers, and D. Dubé, "Mechanical properties and microstructure of new magnesium—lithium base alloys," *Materials Science and Engineering: A*, vol. 220, no. 1, pp. 69–77, Dec. 1996, doi: 10.1016/S0921-5093(96)10460-3.

[2] T.-C. Chang, J.-Y. Wang, C.-L. Chu, and S. Lee, "Mechanical properties and microstructures of various Mg–Li alloys," *Materials Letters*, vol. 60, no. 27, pp. 3272–3276, Nov. 2006, doi: 10.1016/j.matlet.2006.03.052.

[3] H. Haferkamp, M. Niemeyer, R. Boehm, U. Holzkamp, C. Jaschik, and V. Kaese, "Development, Processing and Applications Range of Magnesium Lithium Alloys," *Materials Science Forum*, vol. 350–351, pp. 31–42, 2000, doi: 10.4028/www.scientific.net/MSF.350-351.31.

[4] A. Białobrzeski, K. Saja, and K. Hubner, "Ultralight Magnesium-Lithium Alloys," *undefined*, 2007, Accessed: Aug. 26, 2021. [Online]. Available: https://www.semanticscholar.org/paper/Ultralight-Magnesium-Lithium-Alloys-Bia%C5%82obrzeski-Saja/a9d7abb37af2b6b011e298fd37c423b184a3038c

[5] "Magnesium Elektron WE43 Alloy (UNS M18430)," *AZoM.com*, Jun. 18, 2013. https://www.azom.com/article.aspx?ArticleID=9279 (accessed Aug. 19, 2021).

[6] P. S. says, "Magnesium AZ31B Alloy (UNS M11311)," *AZoM.com*, Sep. 04, 2012. https://www.azom.com/article.aspx?ArticleID=6707 (accessed Aug. 19, 2021).

[7] "Magnesium ZK60A Alloy (M16600)," *AZoM.com*, Sep. 04, 2012. https://www.azom.com/article.aspx?ArticleID=6710 (accessed Aug. 19, 2021).

[8] H. Matsunoshita, K. Edalati, M. Furui, and Z. Horita, "Ultrafine-grained magnesium–lithium alloy processed by high-pressure torsion: Low-temperature superplasticity and potential for hydroforming," *Materials Science and Engineering: A*, vol. 640, pp. 443–448, Jul. 2015, doi: 10.1016/j.msea.2015.05.103.

[9] Q. Su *et al.*, "Microstructural Evolution and Mechanical Properties in Superlight Mg-Li Alloy Processed by High-Pressure Torsion," *Materials*, vol. 11, no. 4, Art. no. 4, Apr. 2018, doi: 10.3390/ma11040598.

[10] K. Edalati *et al.*, "Ultra-severe plastic deformation: Evolution of microstructure, phase transformation and hardness in immiscible magnesium-based systems," *Materials Science and Engineering: A*, vol. 701, pp. 158–166, Jul. 2017, doi: 10.1016/j.msea.2017.06.076.

[11] T. Mineta, K. Hasegawa, and H. Sato, “High strength and plastic deformability of Mg–Li–Al alloy with dual BCC phase produced by a combination of heat treatment and multi-directional forging in channel die,” *Materials Science and Engineering: A*, vol. 773, p. 138867, Jan. 2020, doi: 10.1016/j.msea.2019.138867.

[12] S. Li, L. Chen, J. Tang, G. Zhao, and C. Zhang, “Microstructure and mechanical properties of hot extruded Mg-8.89Li-0.96Zn alloy,” *Results in Physics*, vol. 13, p. 102148, Jun. 2019, doi: 10.1016/j.rinp.2019.02.084.

[13] Y. Wang *et al.*, “Microstructure and mechanical properties of ultra-lightweight Mg-Li-Al/Al-Li composite produced by accumulative roll bonding at ambient temperature,” *Materials Science and Engineering: A*, vol. 787, p. 139494, Jun. 2020, doi: 10.1016/j.msea.2020.139494.

[14] Q.-Y. Che *et al.*, “Microstructure and mechanical properties of magnesium–lithium alloy prepared by friction stir processing,” *Rare Met.*, vol. 40, no. 9, pp. 2552–2559, Sep. 2021, doi: 10.1007/s12598-019-01217-2.

[15] J. Dutkiewicz *et al.*, “Effect of KOBO Extrusion and Following Cyclic Forging on Grain Refinement of Mg–9Li–2Al–0.5Sc Alloy,” *Met. Mater. Int.*, vol. 26, no. 7, pp. 1004–1014, Jul. 2020, doi: 10.1007/s12540-019-00350-y.

[16] Z. Wang *et al.*, “Microstructure and Mechanical Properties of a Two-Phase Mg–Li Alloy Processed By Constrained Groove Pressing,” *Advanced Engineering Materials*, vol. 23, 2021, doi: 10.1002/adem.202000614.

[17] W. J. Kim, M. J. Kim, and J. Y. Wang, “Ultrafine-grained Mg–9Li–1Zn alloy sheets exhibiting low temperature superplasticity,” *Materials Science and Engineering: A*, vol. 516, no. 1, pp. 17–22, Aug. 2009, doi: 10.1016/j.msea.2009.03.089.

[18] Y. Yang *et al.*, “Effects of annealing temperature on microstructure and mechanical properties of LZ91 alloy,” *Materials Science and Technology*, vol. 36, no. 18, pp. 2010–2017, Dec. 2020, doi: 10.1080/02670836.2020.1853361.

[19] J. Guo, J. Wang, T. Zhang, and S. Zhang, “Microstructure and properties of LZ91 magnesium alloy processed by asynchronous accumulative roll bonding,” *Mater. Res. Express*, vol. 7, no. 12, p. 126513, Dec. 2020, doi: 10.1088/2053-1591/abd068.

[20] S. S. Nene, B. P. Kashyap, N. Prabhu, Y. Estrin, and T. Al-Samman, “Microstructure refinement and its effect on specific strength and bio-corrosion resistance in ultralight Mg–4Li–1Ca (LC41) alloy by hot rolling,” *Journal of Alloys and Compounds*, vol. 615, pp. 501–506, Dec. 2014, doi: 10.1016/j.jallcom.2014.06.151.

[21] J. Dutkiewicz, S. Rusz, W. Maziarz, W. Skuza, D. Kuc, and O. Hilser, "Modification of Microstructure and Properties of Extruded Mg-Li-Al Alloys of α and α+ β Phase Composition using ECAP Processing," *Acta Phys. Pol. A*, vol. 131, no. 5, pp. 1303–1307, May 2017, doi: 10.12693/APhysPolA.131.1303.

[22] P. Minárik, R. Král, J. Čížek, and F. Chmelík, "Effect of different c/a ratio on the microstructure and mechanical properties in magnesium alloys processed by ECAP," *Acta Materialia*, vol. 107, pp. 83–95, Apr. 2016, doi: 10.1016/j.actamat.2015.12.050.

[23] M. Zhou, Y. Morisada, H. Fujii, and J.-Y. Wang, "Pronounced low-temperature superplasticity of friction stir processed Mg–9Li–1Zn alloy," *Materials Science and Engineering: A*, vol. 780, p. 139071, Apr. 2020, doi: 10.1016/j.msea.2020.139071.

[24] H. Somekawa and C. A. Schuh, "Effect of solid solution elements on nanoindentation hardness, rate dependence, and incipient plasticity in fine grained magnesium alloys," *Acta Materialia*, vol. 59, no. 20, pp. 7554–7563, Dec. 2011, doi: 10.1016/j.actamat.2011.08.047.

[25] F. Cao, G. Xue, and G. Xu, "Superplasticity of a dual-phase-dominated Mg-Li-Al-Zn-Sr alloy processed by multidirectional forging and rolling," *Materials Science and Engineering: A*, vol. 704, pp. 360–374, Sep. 2017, doi: 10.1016/j.msea.2017.08.037.

[26] F. Guo, L. Liu, Y. Ma, L. Jiang, D. Zhang, and F. Pan, "Mechanism of phase refinement and its effect on mechanical properties of a severely deformed dual-phase Mg–Li alloy during annealing," *Materials Science and Engineering: A*, vol. 772, p. 138792, Jan. 2020, doi: 10.1016/j.msea.2019.138792.

[27] Y. Yang *et al.*, "Achieving ultra-strong Magnesium–lithium alloys by low-strain rotary swaging," *Materials Research Letters*, vol. 9, no. 6, pp. 255–262, Jun. 2021, doi: 10.1080/21663831.2021.1891150.

[28] S. Tang *et al.*, "Precipitation strengthening in an ultralight magnesium alloy," *Nat Commun*, vol. 10, no. 1, p. 1003, Mar. 2019, doi: 10.1038/s41467-019-08954-z.

[29] J. Liao, N. Yamamoto, and K. Nakata, "Effect of Dispersed Intermetallic Particles on Microstructural Evolution in the Friction Stir Weld of a Fine-Grained Magnesium Alloy," *Metall Mater Trans A*, vol. 40, no. 9, pp. 2212–2219, Sep. 2009, doi: 10.1007/s11661-009-9921-2.

[30] P. Cao, L. Lu, and M. O. Lai, "Grain growth and kinetics for nanocrystalline magnesium alloy produced by mechanical alloying," *Materials Research Bulletin*, vol. 36, no. 5, pp. 981–988, Mar. 2001, doi: 10.1016/S0025-5408(01)00578-5.

[31] J. Geng and J. F. Nie, “Microstructure and mechanical properties of extruded Mg–1Ca–1Zn–0.6Zr alloy,” *Materials Science and Engineering: A*, vol. 653, pp. 27–34, Jan. 2016, doi: 10.1016/j.msea.2015.12.004.

[32] K. Edalati *et al.*, “Room-Temperature Superplasticity in an Ultrafine-Grained Magnesium Alloy,” *Sci Rep*, vol. 7, no. 1, p. 2662, Jun. 2017, doi: 10.1038/s41598-017-02846-2.

[33] C. Tian, H. Lu, and L. Zhao, “Microstructure Evolution and Mechanical Properties of Mg-14%Li-1%Al Alloy During the High-Pressure Torsion,” in *Magnesium Technology 2014*, M. Alderman, M. V. Manuel, N. Hort, and N. R. Neelameggham, Eds. Cham: Springer International Publishing, 2016, pp. 167–170. doi: 10.1007/978-3-319-48231-6_34.

[34] R. B. Figueiredo and T. G. Langdon, “Processing Magnesium and Its Alloys by High-Pressure Torsion: An Overview,” *Advanced Engineering Materials*, vol. 21, no. 1, p. 1801039, 2019, doi: 10.1002/adem.201801039.

[35] Y. Huang, R. B. Figueiredo, and T. G. Langdon, “EFFECT OF HPT PROCESSING TEMPERATURE ON,” p. 9.

[36] R. B. Figueiredo and T. G. Langdon, “Grain refinement and mechanical behavior of a magnesium alloy processed by ECAP,” *J Mater Sci*, vol. 45, no. 17, pp. 4827–4836, Sep. 2010, doi: 10.1007/s10853-010-4589-y.

[37] M. Cabibbo, E. Evangelista, and M. Vedani, “Influence of severe plastic deformations on secondary phase precipitation in a 6082 Al-Mg-Si alloy,” *Metall and Mat Trans A*, vol. 36, no. 5, pp. 1353–1364, May 2005, doi: 10.1007/s11661-005-0226-9.

[38] J. M. Cubero-Sesin and Z. Horita, “Mechanical Properties and Microstructures of Al-Fe Alloys Processed by High-Pressure Torsion,” *Metall Mater Trans A*, vol. 43, no. 13, pp. 5182–5192, Dec. 2012, doi: 10.1007/s11661-012-1341-z.

[39] K. Bryła, J. Morgiel, M. Faryna, K. Edalati, and Z. Horita, “Effect of high-pressure torsion on grain refinement, strength enhancement and uniform ductility of EZ magnesium alloy,” *Materials Letters*, vol. 212, pp. 323–326, Feb. 2018, doi: 10.1016/j.matlet.2017.10.113.

[40] Z. Feng, X. Luo, Y. Chen, N. Chen, and G. Wu, “Surface severe plastic deformation induced solute and precipitate redistribution in an Al-Cu-Mg alloy,” *Journal of Alloys and Compounds*, vol. 773, pp. 585–596, Jan. 2019, doi: 10.1016/j.jallcom.2018.09.226.

[41] J. Han, Z. Zhu, H. Li, and C. Gao, “Microstructural evolution, mechanical property and thermal stability of Al–Li 2198-T8 alloy processed by high pressure torsion,” *Materials Science and Engineering: A*, vol. 651, pp. 435–441, Jan. 2016, doi: 10.1016/j.msea.2015.10.112.

[42] B. Srinivasarao, A. P. Zhilyaev, I. Gutiérrez-Urrutia, and M. T. Pérez-Prado, “Stabilization of metastable phases in Mg–Li alloys by high-pressure torsion,” *Scripta Materialia*, vol. 68, no. 8, pp. 583–586, Apr. 2013, doi: 10.1016/j.scriptamat.2012.12.008.

[43] W. T. Sun *et al.*, “Exceptional grain refinement in a Mg alloy during high pressure torsion due to rare earth containing nanosized precipitates,” *Materials Science and Engineering: A*, vol. 728, pp. 115–123, Jun. 2018, doi: 10.1016/j.msea.2018.05.021.

[44] P. Fei, Z. Qu, and R. Wu, “Microstructure and hardness of Mg–9Li–6Al–xLa (x=0, 2, 5) alloys during solid solution treatment,” *Materials Science and Engineering: A*, vol. 625, pp. 169–176, Feb. 2015, doi: 10.1016/j.msea.2014.12.014.

[45] C. L. P. Silva, I. C. Tristão, S. Sabbaghianrad, S. A. Torbati-Sarraf, R. B. Figueiredo, and T. G. Langdon, “Microstructure and Hardness Evolution in Magnesium Processed by HPT,” *Mat. Res.*, vol. 20, no. suppl 1, pp. 2–7, Sep. 2017, doi: 10.1590/1980-5373-mr-2017-0223.

[46] C. L. P. Silva, R. B. Soares, P. H. R. Pereira, R. B. Figueiredo, V. F. C. Lins, and T. G. Langdon, “The Effect of High-Pressure Torsion on Microstructure, Hardness and Corrosion Behavior for Pure Magnesium and Different Magnesium Alloys,” *Advanced Engineering Materials*, vol. 21, no. 3, p. 1801081, 2019, doi: 10.1002/adem.201801081.

[47] K. Edalati, A. Yamamoto, Z. Horita, and T. Ishihara, “High-pressure torsion of pure magnesium: Evolution of mechanical properties, microstructures and hydrogen storage capacity with equivalent strain,” *Scripta Materialia*, vol. 64, no. 9, pp. 880–883, May 2011, doi: 10.1016/j.scriptamat.2011.01.023.

[48] B. Sułkowski, M. Janoska, G. Boczkal, R. Chulist, M. Mroczkowski, and P. Pałka, “The effect of severe plastic deformation on the Mg properties after CEC deformation,” *Journal of Magnesium and Alloys*, vol. 8, no. 3, pp. 761–768, Sep. 2020, doi: 10.1016/j.jma.2020.04.005.

[49] S. Biswas, S. Singh Dhinwal, and S. Suwas, “Room-temperature equal channel angular extrusion of pure magnesium,” *Acta Materialia*, vol. 58, no. 9, pp. 3247–3261, May 2010, doi: 10.1016/j.actamat.2010.01.051.

[50] D. Ahmadkhaniha *et al.*, “Effect of high-pressure torsion on microstructure, mechanical properties and corrosion resistance of cast pure Mg,” *J Mater Sci*, vol. 53, no. 24, pp. 16585–16597, Dec. 2018, doi: 10.1007/s10853-018-2779-1.

[51] L. R. C. Malheiros, R. B. Figueiredo, and T. Langdon, “Processing Different Magnesium Alloys through HPT,” *Materials Science Forum*, vol. 783–786, pp. 2617–2622, 2014, doi: 10.4028/www.scientific.net/MSF.783-786.2617.

[52] G. Ji, Y. Xiaohui, N. Song, and S. Min, “Structural and Hardness Evolution of Pure Magnesium Subjected to High Pressure Torsion,” *Rare Metal Materials and Engineering*, vol. 47, no. 5, pp. 1347–1351, May 2018, doi: 10.1016/S1875-5372(18)30133-4.

[53] X. G. Qiao *et al.*, “Hardening mechanism of commercially pure Mg processed by high pressure torsion at room temperature,” *Materials Science and Engineering: A*, vol. 619, pp. 95–106, Dec. 2014, doi: 10.1016/j.msea.2014.09.068.

[54] N. Li, Y. D. Li, Y. X. Li, Y. H. Wu, Y. F. Zheng, and Y. Han, “Effect of surface mechanical attrition treatment on biodegradable Mg–1Ca alloy,” *Materials Science and Engineering: C*, vol. 35, pp. 314–321, Feb. 2014, doi: 10.1016/j.msec.2013.11.010.

[55] Y. S. Jeong and W. J. Kim, “Enhancement of mechanical properties and corrosion resistance of Mg–Ca alloys through microstructural refinement by indirect extrusion,” *Corrosion Science*, vol. 82, pp. 392–403, May 2014, doi: 10.1016/j.corsci.2014.01.041.

[56] W. Li *et al.*, “*In vitro* and *in vivo* studies on ultrafine-grained biodegradable pure Mg, Mg–Ca alloy and Mg–Sr alloy processed by high-pressure torsion,” *Biomater. Sci.*, vol. 8, no. 18, pp. 5071–5087, 2020, doi: 10.1039/D0BM00805B.

[57] H. K. Kim and W. J. Kim, “Microstructural instability and strength of an AZ31 Mg alloy after severe plastic deformation,” *Materials Science and Engineering: A*, vol. 385, no. 1, pp. 300–308, Nov. 2004, doi: 10.1016/j.msea.2004.06.055.

[58] J. Xu *et al.*, “Microhardness, microstructure and tensile behavior of an AZ31 magnesium alloy processed by high-pressure torsion,” *J Mater Sci*, vol. 50, no. 22, pp. 7424–7436, Nov. 2015, doi: 10.1007/s10853-015-9300-x.

[59] P. Seenuvasaperumal, K. Doi, D. A. Basha, A. Singh, A. Elayaperumal, and K. Tsuchiya, “Wear behavior of HPT processed UFG AZ31B magnesium alloy,” *Materials Letters*, vol. 227, pp. 194–198, Sep. 2018, doi: 10.1016/j.matlet.2018.05.076.

[60] T. Hosaka, S. Yoshihara, I. Amanina, and B. J. MacDonald, “Influence of Grain Refinement and Residual Stress on Corrosion Behavior of AZ31 Magnesium Alloy

Processed by ECAP in RPMI-1640 Medium," *Procedia Engineering*, vol. 184, pp. 432–441, Jan. 2017, doi: 10.1016/j.proeng.2017.04.114.

[61] A. Muralidhar, S. Narendranath, and H. Shivananda Nayaka, "Effect of equal channel angular pressing on AZ31 wrought magnesium alloys," *Journal of Magnesium and Alloys*, vol. 1, no. 4, pp. 336–340, Dec. 2013, doi: 10.1016/j.jma.2013.11.007.

[62] J. Suh, J. Victoria-Hernández, D. Letzig, R. Golle, and W. Volk, "Effect of processing route on texture and cold formability of AZ31 Mg alloy sheets processed by ECAP," *Materials Science and Engineering: A*, vol. 669, pp. 159–170, Jul. 2016, doi: 10.1016/j.msea.2016.05.027.

[63] J. Stráská, M. Janeček, J. Gubicza, T. Krajňák, E. Y. Yoon, and H. S. Kim, "Evolution of microstructure and hardness in AZ31 alloy processed by high pressure torsion," *Materials Science and Engineering: A*, vol. 625, pp. 98–106, Feb. 2015, doi: 10.1016/j.msea.2014.12.005.

[64] Y. Huang, R. B. Figueiredo, T. Baudin, F. Brisset, and T. G. Langdon, "Evolution of Strength and Homogeneity in a Magnesium AZ31 Alloy Processed by High-Pressure Torsion at Different Temperatures," *Advanced Engineering Materials*, vol. 14, no. 11, pp. 1018–1026, 2012, doi: 10.1002/adem.201200016.

[65] T. Masuda and Z. Horita, "Grain Refinement of AZ31 and AZ61 Mg Alloys through Room Temperature Processing by UP-Scaled High-Pressure Torsion," *Materials Transactions*, vol. 60, no. 7, pp. 1104–1110, 2019, doi: 10.2320/matertrans.M2018308.

[66] A. Tehranchi, B. Yin, and W. A. Curtin, "Solute strengthening of basal slip in Mg alloys," *Acta Materialia*, vol. 151, pp. 56–66, Jun. 2018, doi: 10.1016/j.actamat.2018.02.056.

[67] Z. R. Liu and D. Y. Li, "The electronic origin of strengthening and ductilizing magnesium by solid solutes," *Acta Materialia*, vol. 89, pp. 225–233, May 2015, doi: 10.1016/j.actamat.2015.01.051.

[68] R. Zheng, J.-P. Du, S. Gao, H. Somekawa, S. Ogata, and N. Tsuji, "Transition of dominant deformation mode in bulk polycrystalline pure Mg by ultra-grain refinement down to sub-micrometer," *Acta Materialia*, vol. 198, pp. 35–46, Oct. 2020, doi: 10.1016/j.actamat.2020.07.055.

[69] M. M. Castro, P. H. R. Pereira, A. Isaac, T. G. Langdon, and R. B. Figueiredo, "Inverse Hall–Petch Behaviour in an AZ91 Alloy and in an AZ91–Al2O3 Composite Consolidated by High-Pressure Torsion," *Advanced Engineering Materials*, vol. 22, no. 10, p. 1900894, 2020, doi: 10.1002/adem.201900894.

[70] H. Somekawa and T. Mukai, “Effect of grain boundary structures on grain boundary sliding in magnesium,” *Materials Letters*, vol. 76, pp. 32–35, Jun. 2012, doi: 10.1016/j.matlet.2012.02.010.

[71] H. Somekawa and T. Mukai, “Hall–Petch Breakdown in Fine-Grained Pure Magnesium at Low Strain Rates,” *Metall and Mat Trans A*, vol. 46, no. 2, pp. 894–902, Feb. 2015, doi: 10.1007/s11661-014-2641-2.

[72] Z. C. Cordero, B. E. Knight, and C. A. Schuh, “Six decades of the Hall–Petch effect – a survey of grain-size strengthening studies on pure metals,” *International Materials Reviews*, vol. 61, no. 8, pp. 495–512, Nov. 2016, doi: 10.1080/09506608.2016.1191808.

[73] V. Bata and E. V. Pereloma, “An alternative physical explanation of the Hall–Petch relation,” *Acta Materialia*, vol. 52, no. 3, pp. 657–665, Feb. 2004, doi: 10.1016/j.actamat.2003.10.002.

[74] A. H. Chokshi, A. Rosen, J. Karch, and H. Gleiter, “On the validity of the hall-petch relationship in nanocrystalline materials,” *Scripta Metallurgica*, vol. 23, no. 10, pp. 1679–1683, Oct. 1989, doi: 10.1016/0036-9748(89)90342-6.

[75] B. Mintz, “Importance of k_y (Hall-Petch slope) in determining strength of steels,” *Metals Technology*, vol. 11, no. 1, pp. 265–272, Jan. 1984, doi: 10.1179/030716984803274693.

[76] H. L. Kim, J. S. Park, and Y. W. Chang, “Effects of lattice parameter changes on critical resolved shear stress and mechanical properties of magnesium binary single crystals,” *Materials Science and Engineering: A*, vol. 540, pp. 198–206, Apr. 2012, doi: 10.1016/j.msea.2012.01.126.

[77] W. B. Hutchinson and M. R. Barnett, “Effective values of critical resolved shear stress for slip in polycrystalline magnesium and other hcp metals,” *Scripta Materialia*, vol. 63, no. 7, pp. 737–740, Oct. 2010, doi: 10.1016/j.scriptamat.2010.05.047.

[78] G. Zhu *et al.*, “Improving ductility of a Mg alloy via non-basal slip induced by Ca addition,” *International Journal of Plasticity*, vol. 120, pp. 164–179, Sep. 2019, doi: 10.1016/j.ijplas.2019.04.020.

[79] K.-H. Kim, J. H. Hwang, H.-S. Jang, J. B. Jeon, N. J. Kim, and B.-J. Lee, “Dislocation binding as an origin for the improvement of room temperature ductility in Mg alloys,” *Materials Science and Engineering: A*, vol. 715, pp. 266–275, Feb. 2018, doi: 10.1016/j.msea.2018.01.010.

[80] E. Nembach, “The dependence of the hall-petch slope on the γ′ -precipitate dispersion of polycrystals of a nickel-base superalloy,” *Scripta Metallurgica et Materialia*, vol. 24, no. 4, pp. 787–792, Apr. 1990, doi: 10.1016/0956-716X(90)90243-A.

[81] C. L. Li, Q. S. Mei, J. Y. Li, F. Chen, Y. Ma, and X. M. Mei, “Hall-Petch relations and strengthening of Al-ZnO composites in view of grain size relative to interparticle spacing,” *Scripta Materialia*, vol. 153, pp. 27–30, Aug. 2018, doi: 10.1016/j.scriptamat.2018.04.042.

[82] N. Hansen, “Strengthening of aluminium by a three-dimensional network of aluminium-oxide particles,” *Acta Metallurgica*, vol. 17, no. 5, pp. 637–642, May 1969, doi: 10.1016/0001-6160(69)90123-0.

[83] Y. S. Sato, M. Urata, H. Kokawa, and K. Ikeda, “Hall–Petch relationship in friction stir welds of equal channel angular-pressed aluminium alloys,” *Materials Science and Engineering: A*, vol. 354, no. 1, pp. 298–305, Aug. 2003, doi: 10.1016/S0921-5093(03)00008-X.

[84] H. Yu, Y. Xin, M. Wang, and Q. Liu, “Hall-Petch relationship in Mg alloys: A review,” *Journal of Materials Science & Technology*, vol. 34, no. 2, pp. 248–256, Feb. 2018, doi: 10.1016/j.jmst.2017.07.022.

[85] J.-S. Leu, C.-T. Chiang, S. Lee, Y.-H. Chen, and C.-L. Chu, “Strengthening and Room Temperature Age-Softening of Super-Light Mg-Li Alloys,” *J. of Materi Eng and Perform*, vol. 19, no. 9, pp. 1235–1239, Dec. 2010, doi: 10.1007/s11665-010-9606-4.

Chapter 5 - Conclusions

Magnesium alloys have potential to expand the space of light-weight structural materials, especially if the poor bulk strength and thermal stability can be overcome. Within this dissertation, the underlying mechanisms contributing to strengthening and thermal stability in magnesium systems as they relate to fine grain sizes and second-phase particles is examined. In order to do this, three studies were included as written for publication that, together, address the following questions:

1. How can transitions in deformation mechanisms affecting strength be incorporated into conventional strengthening models?
2. What role do secondary phases play in stabilization of grain sizes and strengthening in fine-grained magnesium?

Chapter 2 discussed the evaluation of texture intensity in a hot-rolled Mg-RE alloy containing nano-spaced stacking faults. A previous study had proposed the extreme strengthening to be resultant from the stacking faults, however, the role of texture, which is typically strong in rolled magnesium, was not evaluated and could not be discounted as a significant contribution to overall strength. The results of the texture analysis show that the texture in this system is weak relative to other rolled magnesium systems that exhibit significant strengthening due to increased basal texture intensity. The weak texture was unexpected and concluded to be due to the rare-earth alloying additions and static recrystallization.

The rare-earth additions lowered the stacking fault energy of the system, lowering the critical resolved shear stress required to activate harder slip systems, and lessening the

driving force for the grains to reorient to accommodate slip during rolling. While dynamic recrystallization occurring during deformation to nucleate new grains and orient grains to accommodate the imposed strain which increase texture intensity, static recrystallization causes texture intensity weakening as grains are not constrained for strain accommodation. The author of the previous study on hot-rolled Mg-RE with nano-spaced stacking faults proposed a physical model to describe the strengthening effect which relates the yield stress to the inverse spacing of the stacking fault in a similar fashion to the Hall-Petch relation. What is interesting about this, however, is that the linear trend does not deviate even at small stacking fault spacings, whereas the Hall-Petch trend has been experimentally shown to break down below a critical grain size.

Chapter 3 talks to this Hall-Petch breakdown in more detail as a Mg-YH2 metal-matrix composite with grain sizes from 1-4μm was used to demonstrate the disparity that arises between estimated strengths when using the current models that do not account for this Hall-Petch breakdown and inversion trend. The common strengthening models load bearing, CTE-EM mismatch, Orowan, and Hall-Petch were evaluated for this system and the estimated strength was compared to experimental results. The models show a majority strength contribution from Hall-Petch strengthening, with a small amount of strengthening from Orowan, and negligible contributions from load bearing or CTE-EM mismatch. The Hall-Petch model was evaluated two ways: first using a normal Hall-Petch trend, and second by applying Hall-Petch breakdown and inverted coefficients. It was found that by accounting for the breakdown and inversion in the Hall-Petch model depending on grain size, the experimental results matched more closely to the predicted

results. Sources of variability in the calculations made in this study include Hall-Petch coefficient selection, and comparison of yield strength estimates using a Tabor's estimate from hardness data. Regardless, this paper demonstrated the need to account for the Hall-Petch breakdown in magnesium-based metal-matrix composites to more accurately predict strength using models.

Extending this study, chapter 4 goes into strengthening in a fine-grained magnesium alloy with enhanced thermal stability. A Mg-Li-Ca alloy processed by HPT achieved sub-micron grain sizes leading to hardness up to 92HV, on the high end when compared to other Mg-Li alloys and to many other Mg-based alloys as a whole. This strengthening is due to the fine grains achieved during HPT, and to the fine, dispersed second-phase Mg_2Ca particles contributing to dispersion strengthening. These particles also act to stabilize grains by Zener pinning and grain boundary drag to retain improved hardness properties up to 150°C when subjected to annealing treatments. This finding is a significant improvement over other Mg-Li systems which exhibit destabilization at room temperature or slightly elevated temperatures.

From these studies, in order to advance an understanding of strengthening mechanisms as a function of domain size and secondary phases, the questions posed in the introduction and were addressed.

First, how can transitions in deformation mechanisms affecting strength be incorporated into conventional strengthening models? In chapter 3 we saw that for magnesium-based metal-matrix composites, Hall-Petch strengthening is typically the significant mechanism, and in a system possessing grainsizes where the typical Hall-

Petch regime breaks down, the conventional Hall-Petch model is insufficient. Instead, a variation of the Hall-Petch model can be used where the Hall-Petch coefficient used is dependent on the grain size of the system. There is still room for refinement of these models, and considering the plethora of factors that affect the Hall-Petch coefficient, this model will not extend well to systems with multiple significant strengthening mechanisms at play at once.

Secondly, what is the role that secondary phases play in stabilization of grain sizes and strengthening in a fine-grained magnesium alloy? Chapter 4 covered a sub-micron Mg-Li-Ca alloy where it was shown that Hall-Petch strengthening and dispersion strengthening contributed to the high hardness values seen. The system also retained the fine microstructure and hardness up to 150°C when annealed, showing that the secondary phase particles act as stabilizers along grain boundaries through Zener pinning, and retard grain boundary motion through drag.

Together, these studies provide a step towards understanding the complicated nature of strengthening mechanisms as they are affected across grain size domains in magnesium. Future work can be done in refining the strengthening models applied to fine-grained magnesium systems that better encompass the transition of deformation modes as they relate to strengthening. Work can also be done in the realm of the strength-ductility paradox where a combination of ultra-fine-grained magnesium and a critical volume of secondary phase dispersions will allow for enhanced ductility by allowing some grain boundary sliding to occur, and yet retention of microstructure and strength as the secondary phase particle pin a fraction of boundaries, preventing sliding.